Spontaneous mirror parity violation, common origin of matter and dark matter, and the LHC signatures

Jian-Wei Cui,[1] Hong-Jian He,[1,2,3] Lan-Chun Lü,[1] and Fu-Rong Yin[1]

[1]*Institute of Modern Physics and Center for High Energy Physics, Tsinghua University, Beijing 100084, China*
[2]*Center for High Energy Physics, Peking University, Beijing 100871, China*
[3]*Kavli Institute for Theoretical Physics China, Chinese Academy of Sciences, Beijing 100190, China*

(Received 24 November 2011; published 22 May 2012)

Existence of a mirror world in the Universe is a fundamental way to restore the observed parity violation in weak interactions and provides the lightest mirror nucleon as a unique GeV-scale dark matter particle candidate. The visible and mirror worlds share the same spacetime of the Universe and are connected by a unique space-inversion symmetry—the mirror parity (P). We conjecture that the mirror parity is respected by the fundamental interaction Lagrangian, and study its spontaneous breaking from minimizing the Higgs vacuum potential. The domain-wall problem is resolved by a unique soft-breaking linear term from the P-odd weak-singlet Higgs field. We also derive a constraint from big-bang nucleosynthesis. We then analyze the neutrino seesaw for both visible and mirror worlds, and demonstrate that the desired amounts of visible matter and mirror dark matter in the Universe arise from a common origin of CP violation in the neutrino sector via leptogenesis. We derive the Higgs mass spectrum and Higgs couplings with gauge bosons and fermions. We show their consistency with the direct Higgs searches and the indirect precision constraints. We further study the distinctive signatures of the predicted nonstandard Higgs bosons at the LHC. Finally, we analyze the direct detections of GeV-scale mirror dark matter by the TEXONO and CDEX experiments.

DOI: 10.1103/PhysRevD.85.096003 PACS numbers: 11.30.Er, 11.30.Qc, 95.35.+d, 14.60.Pq

I. INTRODUCTION

The experimental fact that weak force in our visible world only invokes left-handed fermions does not necessarily imply the parity violation in the whole Universe. The possible existence of a hidden mirror world in the Universe as a fundamental way of restoring parity was first conceived by Lee and Yang in their seminal work in 1956 [1]. This truly simple and beautiful idea was further developed by several groups in the following decades [2–4], where a mirror parity was introduced to connect the visible and mirror worlds.

On the other hand, astronomy and cosmology observations have pointed to the existence of mystery dark matter which constitutes about 23% of the total energy density of the present Universe. This is 5 times larger than all the visible matter, $\Omega_{\rm DM}$:$\Omega_{\rm B} \simeq 5$:1, but they are still *comparable* within 1 order of magnitude. In parallel to the visible world, the mirror world conserves mirror baryon number and thus protects the stability of the lightest mirror nucleon, providing a natural GeV-scale dark matter candidate [4–7]. This raises an intriguing possibility that the right amount of dark matter is generated via the mirror leptogenesis under a mirror neutrino seesaw, in the same way that the visible matter is generated via ordinary leptogenesis [8,9].

In this work, we will demonstrate that the mirror parity (P) can play a key role to quantitatively connect the visible and mirror neutrino seesaws, including the associated CP violations. We conjecture that *the mirror parity is respected by the fundamental interaction Lagrangian*, so its violation only arises from spontaneous breaking of the Higgs vacuum, and the possible soft breaking can only be linear or bilinear terms; we further conjecture that *all possible soft breakings of mirror parity simply arise from the gauge-singlet sector.* With this conceptually simple and attractive conjecture, we will present a minimal model with spontaneous mirror parity violation, and the domain-wall problem is evaded by a unique soft-breaking term in the singlet Higgs sector. This is unlike most previous studies, where the mirror parity is assumed to be unbroken [4,10]. With this we can realize both the visible and dark matter geneses from a common origin of CP violation in neutrino seesaws via leptogenesis, as ensured by mirror parity between the two neutrino sectors. Our minimal Higgs potential can generate spontaneous mirror parity violation in the weak interaction, where the visible and mirror Higgs bosons develop different vacuum expectation values (VEVs). Our neutrino seesaw sector has another unique soft-breaking term with unequal masses of visible and mirror singlet heavy Majorana neutrinos. These will make the masses of mirror particles differ from the corresponding visible particles in the standard model (SM), and also will cause a different efficiency factor of out-of-equilibrium decays for the heavy singlet mirror neutrinos. We then demonstrate how the right amount of visible and dark matter can be generated from a common origin of CP violation.

Our model has two self-contained seesaw sectors, the visible seesaw and mirror seesaw, with the corresponding visible and mirror singlet Majorana neutrinos. It is the mirror parity that plays the key role to quantitatively

connect the two seesaws (including the exactly equal *CP* phases) and thus ensures the common origin of generating the right amount of visible and mirror dark matter. We will present systematical analysis of the minimal Higgs potential, and quantitatively realize the spontaneous breaking of both the mirror parity and the electroweak gauge symmetry. The mirror Higgs VEV is found to be about a factor of 2 smaller than the visible Higgs VEV. We then derive the distinctive mass spectrum of Higgs bosons and their couplings, leading to new collider phenomenology, different from all previous mirror-model signals. We also analyze the existing low-energy constraints via electroweak precision measurements and direct production. We further study the new signatures of predicted nonstandard Higgs bosons at the LHC. Finally, we analyze the direct detections of mirror dark matter. Our construction also fully differs from a recent interesting study [7] with resonant leptogenesis for the matter and dark-matter genesis, where the visible and mirror sectors share the same right-handed neutrinos with inverse seesaw. The ratio $\Omega_{\rm DM}/\Omega_{\rm B} \simeq 5$ arises from an assumed large ratio (about 1000) [7] of the two VEVs for the mirror and visible Higgs bosons which causes the mirror nucleon about a factor of 5 heavier than the visible nucleon. Two Higgs doublets and one Higgs triplet with soft mirror parity breaking are introduced for both sectors [7], which will generate a mass $\sim$50 MeV for mirror photons and masses $\gtrsim$ 100 MeV for light mirror neutrinos. The existence of proper Higgs potential and its minimum are assumed in [7].

This paper is organized as follows. In Sec. II, we show that a unique mirror parity can be introduced to connect the visible and mirror worlds, as a fundamental way to restore the parity in weak interactions. We then construct a minimal Higgs potential and derive conditions for its physical vacuum to realize both the spontaneous mirror parity violation and spontaneous electroweak symmetry breaking. In Sec. III, we analyze the visible and mirror leptogeneses via neutrino seesaws, with a common origin of *CP* violations. We then derive the conditions for generating the right amount of visible and mirror dark matter. In Sec. IV, we study the analytical structure of the vacuum Higgs potential, and then present three numerical samples for the Higgs vacuum and the corresponding Higgs mass spectrum that obey the conditions for desired matter and dark matter geneses. We further demonstrate their consistency with the current low-energy precision constraints. In Sec. V, we study the distinctive collider signatures of the nonstandard Higgs bosons at the LHC. We further analyze the direct detections of GeV-scale mirror dark matter by the TEXONO [11] and CDEX [12] experiments in Sec. VI. Finally, we conclude in Sec. VII.

II. SPONTANEOUS MIRROR PARITY VIOLATION

In Sec. II, we will first analyze the structure of the mirror model with unbroken mirror parity, and then we discuss the connections between the visible and mirror worlds in Sec. II. We conjecture that *the mirror parity is respected by the fundamental interaction Lagrangian*, so its violation only arises from spontaneous breaking of the Higgs vacuum, and the possible soft breaking can only be linear or bilinear terms; we further conjecture that *all possible soft breakings simply arise from the gauge-singlet sector alone*. With this conceptually simple and attractive conjecture, we will present a minimal model with spontaneous mirror parity violation (Sec. III), where the Higgs sector includes the SM Higgs doublet, the mirror Higgs doublet, and a P-odd weak singlet scalar. We find that the possible soft breakings can be uniquely realized via the P-odd weak singlet scalar in the Higgs potential and via the Majorana mass terms of heavy singlet neutrinos in the seesaw sector. As we will show, the unique soft breaking in Higgs potential nicely evades the domain-wall problem [13] associated with spontaneous mirror parity violation (Sec. II), and the unique soft breaking in the heavy Majorana mass term will play a key role to realize the desired dark matter density (Secs. III).

A. Structure of the model

The visible and mirror worlds share the same spacetime of the Universe, and this leads to a unique space-inversion symmetry—the mirror parity. We know that the representations of Lorentz group can be characterized by $SU(2) \otimes SU(2)$ with generators $A_i = \frac{1}{2}(J_i + iK_i)$ and $B_i = \frac{1}{2}(J_i - iK_i)$, $(i, j = 1, 2, 3)$, where J_i is angular momentum and K_i the Lorentz boost. So each representation is labeled by two angular momenta (j, j'), corresponding to A and B, respectively. Under the parity transformation $\mathcal{P}$, we have $\mathcal{P}J_i\mathcal{P}^{-1} = J_i$ and $\mathcal{P}K_i\mathcal{P}^{-1} = -K_i$. This means the exchange $A_i \leftrightarrow B_i$, i.e., the parity operator transforms a representation (j, j') into (j', j). In the SM, the left-handed fermions belong to $(\frac{1}{2}, 0)$ and group into $SU(2)_L$ doublets, while the right-handed fermions belong to $(0, \frac{1}{2})$ and are $SU(2)_L$ singlets. Hence the parity symmetry is explicitly broken in the SM by the weak interaction.

There are two fundamental ways to restore parity symmetry. One is to enlarge the weak gauge group $SU(2)_L$ into a left-right symmetric form, $SU(2)_L \otimes SU(2)_R$. Assigning the left-handed fermions to $SU(2)_L$ doublets (but $SU(2)_R$ singlets), and right-handed fermions to $SU(2)_R$ doublets (but $SU(2)_L$ singlets). Then, assigning $SU(2)_L \leftrightarrow SU(2)_R$ under the parity transformation, one sees that the parity symmetry is restored. Adding the $B - L$ gauge group, one has the gauge group $SU(2)_L \otimes SU(2)_R \otimes U(1)_{B-L}$, which is just the conventional left-right model [14]. Another fundamental way for parity restoration is to enlarge the matter contents of the SM. To be explicit, we can assign that, under the parity transformation, left-handed fermions f_L transform into corresponding new right-handed fermions f'_R, which also group into doublets of a new gauge group $SU(2)'_R$, and the right-handed fermions f_R transform

into corresponding new left-handed fermions f'_L, which are singlets of group $SU(2)'_R$. This means that we should enlarge the SM gauge group $G_{\rm SM} = SU(3)_c \otimes SU(2)_L \otimes U(1)_Y$ to $G_{\rm SM} \otimes G'_{\rm SM}$, where the new gauge group $G'_{\rm SM} = SU(3)'_c \otimes SU(2)'_R \otimes U(1)'_Y$ [4] is a mirror of $G_{\rm SM}$ with identical gauge couplings, under which the matter contents switch their chiralities. Hence, the parity is restored in the Universe where the visible and mirror worlds coexist in the same spacetime.

In fact, the mirror world is a hidden sector of particles and interactions, as a mirror-duplicate of our visible world. The fermionic matter contents of the mirror model can be summarized below,

$$\begin{aligned}
Q_L^i &\sim \Big(3, \quad 2, \quad \tfrac{1}{6}\Big)\big(1, \quad 1, \quad 0\big)', \\
(Q'_R)^i &\sim \big(1, \quad 1, \quad 0\big)\Big(3, \quad 2, \quad \tfrac{1}{6}\Big)', \\
u_R^i &\sim \Big(3, \quad 1, \quad \tfrac{2}{3}\Big)\big(1, \quad 1, \quad 0\big)', \\
(u'_L)^i &\sim \big(1, \quad 1, \quad 0\big)\Big(3, \quad 1, \quad \tfrac{2}{3}\Big)', \\
d_R^i &\sim \Big(3, \quad 1, \quad -\tfrac{1}{3}\Big)\big(1, \quad 1, \quad 0\big)', \\
(d'_L)^i &\sim \big(1, \quad 1, \quad 0\big)\Big(3, \quad 1, \quad -\tfrac{1}{3}\Big)', \\
L_L^i &\sim \Big(1, \quad 2, \quad -\tfrac{1}{2}\Big)\big(1, \quad 1, \quad 0\big)', \\
(L'_R)^i &\sim \big(1, \quad 1, \quad 0\big)\Big(1, \quad 2, \quad -\tfrac{1}{2}\Big)', \\
e_R^i &\sim \big(1, \quad 1, \quad 0\big)\big(1, \quad 1, \quad 0\big)', \\
(e'_L)^i &\sim \big(1, \quad 1, \quad 0\big)\big(1, \quad 1, \quad -1\big)', \\
\nu_R^i &\sim \big(1, \quad 1, \quad 0\big)\big(1, \quad 1, \quad 0\big)', \\
(\nu'_L)^i &\sim \big(1, \quad 1, \quad 0\big)\big(1, \quad 1, \quad 0\big)', \\
\phi &\sim \Big(1, \quad 2, \quad \tfrac{1}{2}\Big)\big(1, \quad 1, \quad 0\big)', \\
\phi' &\sim \big(1, \quad 1, \quad 0\big)\Big(1, \quad 2, \quad \tfrac{1}{2}\Big)',
\end{aligned} \tag{2.1}$$

where i stands for the family index, and the assigned gauge quantum numbers under $G_{\rm SM} \otimes G'_{\rm SM}$ are also given in the parentheses (with hypercharge Y defined via $Q = I_3 + Y$). Since light neutrinos are massive, we have also included the right-handed (left-handed) neutrinos in the visible (mirror) sector, which are gauge singlets of $G_{\rm SM} \otimes G'_{\rm SM}$. So, under the parity operation $(\vec{x}, t) \to (-\vec{x}, t)$, we have the following transformations for fermions, gauge bosons, and Higgs doublets and their mirror partners:

$$\begin{aligned}
&Q_L^i \leftrightarrow (Q'_R)^i, \quad u_R^i \leftrightarrow (u'_L)^i, \quad d_R^i \leftrightarrow (d'_L)^i, \\
&L_L^i \leftrightarrow (L'_R)^i, \quad e_R^i \leftrightarrow (e'_L)^i, \quad \nu_R^i \leftrightarrow (\nu'_L)^i, \\
&G_\mu^\alpha \leftrightarrow (G_\mu^\alpha)', \quad W_\mu^a \leftrightarrow (W_\mu^a)', \quad B_\mu \leftrightarrow B'_\mu, \\
&\phi \leftrightarrow \phi'.
\end{aligned} \tag{2.2}$$

Furthermore, the parity invariance of the interaction Lagrangian requires the same strengths of the corresponding gauge (Yukawa) couplings between the visible and mirror sectors; besides, the heavy Majorana mass matrices for gauge-singlet neutrinos should be equal between the two sectors as well. For our construction, we will further include a P-odd gauge-singlet scalar (Sec. II) to realize spontaneous mirror parity violation, and allow a unique soft-breaking term in the singlet sector of the Higgs potential to evade the domain-wall problem. We will also allow the visible and mirror heavy Majorana mass matrices to be unequal, as another unique soft breaking in the gauge-singlet sector of neutrino seesaw, which will play a key role for realizing the desired dark matter density (Secs. III).

B. Communication between visible and mirror worlds

As we see, the mirror parity symmetry also doubles the particle contents of the SM, but in a much simpler way than what supersymmetry does. All the mirror particles have not been seen so far, because the ''communication'' between visible and mirror worlds is hard. If the mirror parity exactly holds, all mirror particles have the same masses as their SM partners as well as an independent set of gauge interactions (except sharing the gravity force, which is extremely weak at ordinary laboratory scales). So the mirror sector consists of a ''hidden world'' and thus provides a generic dark matter candidate in the Universe [4–6].

Nevertheless, besides gravitational interaction, there are three fundamental ways by which the mirror world can communicate with our visible world: (i) interaction between visible and mirror Higgs doublets; (ii) mass mixings between singlet visible and mirror neutrinos; and (iii) kinetic gauge mixing of $B_\mu - B'_\mu$:

(i) Interaction between visible and mirror Higgs doublets:
Gauge invariance also allows the following quartic interaction term between the visible and mirror Higgs doublets (ϕ and ϕ') [3,15]:

$$\mathcal{L}_{\phi\phi'} = \tilde{\lambda}(\phi^\dagger \phi)(\phi'^\dagger \phi'). \tag{2.3}$$

After the electroweak symmetry breaking in the visible and mirror sectors, (2.3) can induce a mixing between the Higgs boson h and its mirror partner h'. This will then modify the gauge and Yukawa couplings of both h and h', giving rise to distinct signatures at the LHC. As will be shown in the next subsection, our model construction also generates spontaneous mirror parity violation via $\langle\phi\rangle \neq \langle\phi'\rangle$, and thus gives different masses for mirror gauge bosons (W', Z') and all mirror fermions. All these will have important phenomenological consequences, as to be analyzed in Secs. III.

(ii) Mixing between visible and mirror singlet neutrinos:
Since ν_R and ν'_L are pure gauge singlets, we can write down the following dimension-3 Dirac mass term [16]:

$$\mathcal{L}_{\nu\nu'} = \delta m \bar{\nu}_R \nu'_L + \text{H.c.} \tag{2.4}$$

(iii) Kinetic mixing between visible and mirror photons: Since the Abelian field strength tensors $B_{\mu\nu}$ and $B'_{\mu\nu}$ are gauge-invariant, the Lagrangian will generally include the following dimension-4 mixing operator [3,17]:

$$\mathcal{L}_{BB'} = -\frac{\epsilon_0}{2} B^{\mu\nu} B'_{\mu\nu}. \tag{2.5}$$

After electroweak symmetry breaking, this term gives rise to a kinetic mixing between the electromagnetic field strength tensors for visible and mirror photons,

$$\mathcal{L}^{\gamma\gamma'}_{\text{mix}} = -\frac{\epsilon}{2} F^{\mu\nu} F'_{\mu\nu}, \tag{2.6}$$

where $\epsilon = \epsilon_0 \cos^2\theta_W$ and θ_W is the weak mixing angle. (Since the mirror parity requires gauge groups G_{SM} and G'_{SM} to have identical gauge couplings, the weak mixing angle θ_W remains the same for both visible and mirror sectors.) Although this kinetic mixing is not suppressed by known symmetry, an experimental limit can be inferred from the orthopositronium annihilation into mirror orthopositronium, which imposed a tight upper bound [18,19], $\epsilon < 5 \times 10^{-7}$. A more recent measurement of the invisible decay of orthopositronium reduced the upper limit to $\epsilon < 1.55 \times 10^{-7}$ [20]. In 2010, a new experimental proposal planned to reach a sensitivity down to $\epsilon < 4 \times 10^{-9}$ [21]. But we note that this limit only applies to the case where the mirror parity is unbroken, which can generate oscillation between visible and mirror orthopositroniums. Our model predicts spontaneous mirror parity violation, so we will reanalyze the orthopositronium bound in Sec. IV. The operator [18,19] can also induce $Z - Z'$, $\gamma - Z'$, and $Z - \gamma'$ mixings, which are all proportional to the tiny ϵ parameter. Since these mixings invoke the massive gauge bosons in weak interaction, they cause no stronger bounds than the $\gamma - \gamma'$ mixing.

C. Higgs Potential and spontaneous symmetry breaking

We have conjectured that *the mirror parity is respected by the fundamental interaction Lagrangian*, so its violation only arises from spontaneous breaking of the Higgs vacuum, and the possible soft breaking can only be linear or bilinear terms; we further conjecture that *all possible soft breakings simply arise from the gauge-singlet sector alone*. In this subsection, we present a minimal model with spontaneous mirror parity violation, where the Higgs sector includes the SM Higgs doublet, the mirror Higgs doublet, and a P-odd weak singlet scalar. We show that the possible soft breaking can be uniquely realized via the P-odd weak singlet scalar in the Higgs potential, which evades the domain-wall problem.

For the minimal construction, we introduce a weak-singlet real scalar field χ which is P-odd. So, the Higgs sector consists of two Higgs doublets (ϕ and ϕ') and a real singlet (χ). Under the mirror parity, they transform as follows:

$$\phi \leftrightarrow \phi', \qquad \chi \leftrightarrow -\chi. \tag{2.7}$$

Then, we can write down the most general renormalizable form of the minimal Higgs potential V for (ϕ, ϕ', χ), which preserves the gauge group $G_{\text{SM}} \otimes G'_{\text{SM}}$ and the mirror parity P,

$$\begin{aligned} V(\phi, \phi', \chi) = & -\mu_\phi^2(|\phi|^2 + |\phi'|^2) + \lambda_\phi^+(|\phi|^2 \\ & + |\phi'|^2)^2 + \lambda_\phi^-(|\phi|^2 - |\phi'|^2)^2 \\ & - \tfrac{1}{2}\mu_\chi^2\chi^2 + \tfrac{1}{4}\lambda_\chi\chi^4 + \beta_{\chi\phi}\chi(|\phi|^2 \\ & - |\phi'|^2) + \tfrac{1}{2}\lambda_{\chi\phi}\chi^2(|\phi|^2 + |\phi'|^2), \end{aligned} \tag{2.8a}$$

$$\Delta V_{\text{soft}}(\chi) = \beta_\chi \chi, \tag{2.8b}$$

where we also included the allowed soft P-breaking term ΔV_{soft} from the singlet sector, which is unique and must be linear in the gauge-singlet field χ because we have conjectured that all interactions are naturally P-invariant. The Higgs vacuum expectation values are defined as

$$\langle\phi\rangle \equiv \begin{pmatrix} 0 \\ v_\phi \end{pmatrix}, \quad \langle\phi'\rangle \equiv \begin{pmatrix} 0 \\ v_{\phi'} \end{pmatrix}, \quad \langle\chi\rangle \equiv v_\chi. \tag{2.9}$$

As we will see, the $\beta_{\chi\phi}$ term in (2.8a) is the key to realize $v_\phi \neq v_{\phi'}$, and thus generate the spontaneous mirror parity violation. (Some early studies considered spontaneous mirror parity violation via different approaches, such as setting $v_\phi \ll v_{\phi'}$ and assuming the coupling of symmetry-allowed mixing interaction $|\phi|^2|\phi'|^2$ to be highly suppressed down to the level of 10^{-7} [22]. This is not the case for our model.) Then, comparing the operator (2.3) with the $\lambda_{\phi+}$ and $\lambda_{\phi-}$ terms in Eq. (2.8a), we have the relation

$$\tilde{\lambda} = 2(\lambda_\phi^+ - \lambda_\phi^-). \tag{2.10}$$

Since we are considering the spontaneous P violation, we will encounter the domain-wall problem [13] which occurs for spontaneous breaking of a discrete symmetry (such as parity) with scalar fields. In the literature, there are different ways to avoid this problem [23]. We have derived the unique soft P-breaking term (2.8b) as the simplest resolution here to remove the domain-wall problem. This is because Eq. (2.8b) lifts the degenerate vacua of the Higgs potential (2.8a). It is natural to consider the soft breaking to be relatively small, i.e., the dimension-3 coefficient β_χ is in the range $\beta_\chi \ll \mu_\chi^3$.

With (2.8) and (2.9), we infer the full vacuum Higgs potential,

$$\langle \hat{V}(\phi,\phi',\chi)\rangle \equiv \langle V(\phi,\phi',\chi)\rangle + \langle \Delta V_{\rm soft}(\chi)\rangle, \tag{2.11a}$$

$$\begin{aligned}\langle V\rangle =& -\mu_\phi^2(v_\phi^2+v_{\phi'}^2)+\lambda_\phi^+(v_\phi^2+v_{\phi'}^2)^2\\ &+\lambda_\phi^-(v_\phi^2-v_{\phi'}^2)^2-\tfrac{1}{2}\mu_\chi^2 v_\chi^2+\tfrac{1}{4}\lambda_\chi v_\chi^4\\ &+\beta_{\chi\phi}v_\chi(v_\phi^2-v_{\phi'}^2)+\tfrac{1}{2}\lambda_{\chi\phi}v_\chi^2(v_\phi^2+v_{\phi'}^2),\end{aligned} \tag{2.11b}$$

$$\langle \Delta V_{\rm soft}\rangle = \beta_\chi v_\chi. \tag{2.11c}$$

So we see that the full potential $\hat{V}(\phi,\phi',\chi)$ no longer has degenerate vacua,

$$\hat{V}(v_\phi,v_{\phi'},v_\chi)-\hat{V}(v_{\phi'},v_\phi,-v_\chi)=2\beta_\chi v_\chi\neq 0, \tag{2.12}$$

and thus removes the domain-wall problem. The minimal conditions of the vacuum potential give

$$\frac{\partial\langle\hat{V}\rangle}{\partial v_\phi}=0,\qquad \frac{\partial\langle\hat{V}\rangle}{\partial v_{\phi'}}=0,\qquad \frac{\partial\langle\hat{V}\rangle}{\partial v_\chi}=0, \tag{2.13}$$

which lead to the following equations for the nontrivial vacuum:

$$\begin{aligned}&-\mu_\phi^2+2\lambda_\phi^+(v_\phi^2+v_{\phi'}^2)+2\lambda_\phi^-(v_\phi^2-v_{\phi'}^2)+\beta_{\chi\phi}v_\chi\\ &+\tfrac{1}{2}\lambda_{\chi\phi}v_\chi^2=0,\end{aligned} \tag{2.14a}$$

$$\begin{aligned}&-\mu_\phi^2+2\lambda_\phi^+(v_\phi^2+v_{\phi'}^2)-2\lambda_\phi^-(v_\phi^2-v_{\phi'}^2)-\beta_{\chi\phi}v_\chi\\ &+\tfrac{1}{2}\lambda_{\chi\phi}v_\chi^2=0,\end{aligned} \tag{2.14b}$$

$$\begin{aligned}&-\mu_\chi^2 v_\chi+\lambda_\chi v_\chi^3+\beta_{\chi\phi}(v_\phi^2-v_{\phi'}^2)+\lambda_{\chi\phi}v_\chi(v_\phi^2+v_{\phi'}^2)\\ &+\beta_\chi=0.\end{aligned} \tag{2.14c}$$

From the conditions (2.14a) and (2.14b) we immediately deduce

$$v_\phi^2-v_{\phi'}^2=-\frac{\beta_{\chi\phi}}{2\lambda_\phi^-}v_\chi, \tag{2.15a}$$

$$v_\phi^2+v_{\phi'}^2=\frac{\mu_\phi^2-\frac{1}{2}\lambda_{\chi\phi}v_\chi^2}{2\lambda_\phi^+}. \tag{2.15b}$$

Inspecting Eq. (2.15a), we see that the VEV v_χ of the P-odd scalar χ together with its trilinear coupling $\beta_{\chi\phi}$ is the key to generate $v_\phi\neq v_{\phi'}$ and thus the spontaneous mirror parity violation. We further rewrite (2.15a) as

$$\left(\frac{v_{\phi'}}{v_\phi}\right)^2=1+\frac{\beta_{\chi\phi}v_\chi}{2\lambda_\phi^- v_\phi^2}, \tag{2.16}$$

which shows that choosing the ratio $v_{\phi'}/v_\phi=0.1(0.01)$ requires a fine-tuned cancellation down to the level of $10^{-2}(10^{-4})$ on the right-hand-side (RHS). Hence, the naturalness of our parameter space puts a lower limit on this ratio,

$$\frac{v_{\phi'}}{v_\phi}>0.1, \tag{2.17}$$

by allowing the fine-tuned cancellation on the RHS of (2.16) to be better than 1%.

Using (2.14) we can analytically solve the three VEVs in terms of two mass parameters and five couplings in the Higgs potential (2.8a),

$$v_\phi^2=\frac{1}{4}\left(\frac{\mu_\phi^2-\frac{1}{2}\lambda_{\chi\phi}v_\chi^2}{\lambda_\phi^+}-\frac{\beta_{\chi\phi}}{\lambda_\phi^-}v_\chi\right), \tag{2.18a}$$

$$v_{\phi'}^2=\frac{1}{4}\left(\frac{\mu_\phi^2-\frac{1}{2}\lambda_{\chi\phi}v_\chi^2}{\lambda_\phi^+}+\frac{\beta_{\chi\phi}}{\lambda_\phi^-}v_\chi\right), \tag{2.18b}$$

$$v_{\chi 0}^2=2\frac{\lambda_{\chi\phi}\mu_\phi^2-2\lambda_\phi^+\tilde{\mu}_\chi^2}{\lambda_{\chi\phi}^2-4\lambda_\chi\lambda_\phi^+}, \tag{2.18c}$$

where $\tilde{\mu}_\chi^2\equiv\mu_\chi^2+\frac{\beta_{\chi\phi}^2}{2\lambda_\phi^-}$, and in the last equation, $v_{\chi 0}^2$ is derived under the vanishing soft-breaking parameter $\beta_\chi=0$. To include a nonzero β_χ, we can recast (2.14c) into the form

$$c_3 v_\chi^3-c_1 v_\chi-\beta_\chi=0, \tag{2.19a}$$

$$c_3\equiv\frac{\lambda_{\chi\phi}^2}{4\lambda_\phi^+}-\lambda_\chi, \tag{2.19b}$$

$$c_1\equiv\frac{\lambda_{\chi\phi}\mu_\phi^2}{2\lambda_\phi^+}-\frac{\beta_{\chi\phi}^2}{2\lambda_\phi^-}-\mu_\chi^2, \tag{2.19c}$$

where we have made use of (2.15a) and (2.15b). Since $\beta_\chi\ll\mu_\chi^3,\ \mu_\phi^3$, we can solve (2.19) perturbatively to the first nontrivial order,

$$v_\chi=v_{\chi 0}+\frac{\beta_\chi}{2c_1}+O\left(\frac{\beta_\chi^2}{\mu_{\chi,\phi}^6}\right), \tag{2.20}$$

which reduces back to our leading-order solution (2.18c) in the $\beta_\chi\to 0$ limit.

Choosing unitary gauge and physical vacuum, we see that the doublet ϕ (ϕ') contains a (mirror) neutral Higgs boson, while the P-odd χ gives a singlet scalar particle. So denoting $\Phi=(\phi,\phi',\chi)^T$, we can write down the Higgs mass term $\Phi^T\mathcal{M}^2\Phi$, and derive the 3×3 symmetric mass matrix as follows:

$$\mathcal{M}^2=\begin{pmatrix} m_{\phi\phi}^2 & m_{\phi\phi'}^2 & m_{\phi\chi}^2\\ m_{\phi\phi'}^2 & m_{\phi'\phi'}^2 & m_{\phi'\chi}^2\\ m_{\phi\chi}^2 & m_{\phi'\chi}^2 & m_{\chi\chi}^2\end{pmatrix}, \tag{2.21}$$

with the six elements,

$$
\begin{aligned}
m^2_{\phi\phi} &= 4(\lambda^+_\phi + \lambda^-_\phi)v^2_\phi, \\
m^2_{\phi'\phi'} &= 4(\lambda^+_\phi + \lambda^-_\phi)v^2_{\phi'}, \\
m^2_{\chi\chi} &= -\tfrac{1}{2}\mu^2_\chi + \tfrac{3}{2}\lambda_\chi v^2_\chi + \tfrac{1}{2}\lambda_{\chi\phi}(v^2_\phi + v^2_{\phi'}), \\
m^2_{\phi\phi'} &= 4(\lambda^+_\phi - \lambda^-_\phi)v_\phi v_{\phi'}, \\
m^2_{\phi\chi} &= (\lambda_{\chi\phi} v_\chi + \beta_{\chi\phi})v_\phi, \\
m^2_{\phi'\chi} &= (\lambda_{\chi\phi} v_\chi - \beta_{\chi\phi})v_{\phi'},
\end{aligned}
\tag{2.22}
$$

where we have made use of the vacuum solution (2.18) for simplification. In Sec. IV, we will present numerical samples for the vacuum solution (2.18) and derive the physical Higgs mass spectrum from diagonalizing the mass matrix (2.21).

Finally, we comment on the self-interactions of mirror dark matter due to the unbroken mirror electromagnetism which may be a concern for all mirror models with the unbroken mirror Abelian gauge group. As clarified in [24], the MACHO Collaboration [25] found statistically strong evidence for dark matter in the form of invisible star-sized objects [26], which is just what one would expect if a significant amount of mirror dark matter exists in our galaxy. Another survey analyzed stars across the face of M31 and found significant evidence for a population of halo microlensing dark-matter objects, showing a halo mass fraction of $f = 0.29^{+0.30}_{-0.13}$ [27]. This is consistent with the results of the MACHO Collaboration [26]. For dark matter in the form of MACHO, it will not show self-interactions in the bullet cluster. In addition, it is worth noting that although astronomical observations have put nontrivial constraints on the possible long-range self-interactions of the dark matter, they are valid only for the assumed homogeneous dark-matter distributions and thus need not to be directly applicable to the mirror dark matter as it can form nonhomogeneous type of structures [28]. For the bullet cluster, the observations showed that after a collision of two galaxies, the dark matter can pass through each other as if there are no collisions between them. But other observations exist with the opposite implication. For instance, studies on the Abell-520 cluster (also known as MS 0451 + 02) [29] performed the weak-lensing analysis and subsequent comparison with the optical and X-ray properties of the cluster. It was found [29,30] that the massive dark core coincides with the central X-ray emission peak, but is largely devoid of galaxies, indicating certain self-interactions of the dark matter, which may be explained by the mirror dark matter [31]. Astronomers are making further efforts to explore the true natures of dark matter, including unusual clusters such as Abell-520 and the like.

III. COMMON ORIGIN OF MATTER AND DARK MATTER VIA LEPTOGENESIS

In this section we study the generation of visible matter and mirror dark matter from a common origin in neutrino seesaw via leptogenesis. In Sec. III, with the spontaneous mirror parity violation, we derive the ratio of visible and mirror nucleon masses as a function of the VEVs of visible and mirror Higgs bosons. Then, in Sec. III, we connect the visible and mirror leptogeneses, and compute the ratio of visible and mirror baryon asymmetries in terms of the unique soft P-breaking parameter in the neutrino seesaw. We will present two seesaw constructions for both the visible and mirror neutrino sectors, which explicitly realize the common origin of the matter and dark matter geneses. Then, we demonstrate the realization of the astrophysical observation, $\Omega_{\rm DM}$:$\Omega_{\rm M} \simeq 5$:1. Finally, we analyze the consistency of our mirror model with the constraint from big-bang nucleosynthesis in Sec. III, which puts a nontrivial limit on the ratio of the visible and mirror Higgs VEVs.

A. Common origin of visible and dark matter from leptogenesis

Observations reveal our visible world to be exclusively populated with baryonic matter instead of antimatter. The genesis of net baryon asymmetry requires baryon number violating interactions, C and CP violations, and departure from thermal equilibrium [32]. This can be naturally realized via leptogenesis [8,9], where the leptonic CP violations arise from neutrino seesaw and where the out-of-equilibrium decays of the heavy Majorana neutrino into a lepton-Higgs pair and its conjugate produce the lepton-number asymmetry. Because of the electroweak sphaleron process [33], the lepton asymmetry is partially converted into the desired baryon asymmetry and can explain the observed baryon density today [34],

$$\Omega_{\rm B} = 0.0458 \pm 0.0016. \tag{3.1}$$

As shown in (2.2), the mirror parity connects the particle contents of the visible and mirror sectors with one-to-one correspondence. Furthermore, it requires identical gauge (Yukawa) couplings between the two sectors, as well as the same Majorana mass matrix for the gauge-singlet heavy Majorana neutrinos. Thus, it is very natural to generate the baryonic mirror matter-antimatter asymmetry from mirror leptogenesis. With the spontaneous mirror parity violation (Sec. II) and a unique soft breaking in the singlet sector of a neutrino seesaw, we will generate desired mass splittings between the visible and mirror nucleus, as well as a different efficiency factor of out-of-equilibrium decays for the heavy singlet mirror neutrinos, such that the baryonic mirror matter can naturally provide the observed dark matter density in the Universe [34],

$$\Omega_{\rm DM} = 0.229 \pm 0.015, \tag{3.2}$$

which is only about a factor of 5 larger than $\Omega_{\rm B}$. With (3.1) and (3.2), we derive the ratio, $\Omega_{\rm DM}/\Omega_{\rm B} = 5.00 \pm 0.37$, which gives the 2σ limit: $4.26 < \Omega_{\rm DM}/\Omega_{\rm B} < 5.74$. For the mirror model, we have the visible matter density $\Omega_{\rm M} \simeq \Omega_{\rm B}$ and the mirror dark matter density $\Omega_{\rm DM} \simeq \Omega_{\rm B'}$.

With the mirror baryons serving as natural dark matter, we can thus derive the ratio of dark matter density relative to that of visible matter,

$$\frac{\Omega_{\rm DM}}{\Omega_{\rm M}} \simeq \frac{\Omega_{\rm B'}}{\Omega_{\rm B}} = \frac{\mathcal{N}_{\rm B'}}{\mathcal{N}_{\rm B}} \frac{m_{N'}}{m_N}, \tag{3.3}$$

where m_N denotes the visible nucleon mass and $m_{N'}$ the mirror nucleon mass. In (3.3), $\mathcal{N}_{\rm B}$ ($\mathcal{N}_{\rm B'}$) is the baryon number (mirror baryon number) computed in a portion of comoving volume [which contains one photon (mirror photon) before the onset of (mirror) leptogenesis].

As shown in Sec. II, the spontaneous mirror parity violation makes the visible Higgs VEV differ from that of the mirror Higgs, $v_\phi \neq v_{\phi'}$. So, the masses of the visible and mirror nucleus also differ from each other, $m_N \neq m_{N'}$. For further analysis, let us derive the relation between nucleon mass and the Higgs boson VEV. The running of QCD gauge coupling $\alpha_s(\mu)$ is given by

$$\alpha_s(\mu) = \frac{2\pi}{11 - \frac{2}{3}n_f} \frac{1}{\ln(\mu/\Lambda)}, \tag{3.4}$$

while the mirror QCD′ has its running gauge coupling $\alpha'_s(\mu)$ behave as

$$\alpha'_s(\mu) = \frac{2\pi}{11 - \frac{2}{3}n'_f} \frac{1}{\ln(\mu/\Lambda')}, \tag{3.5}$$

where we denote $\Lambda = \Lambda_{\rm QCD}$ for visible QCD and $\Lambda' = \Lambda'_{\rm QCD}$ for mirror QCD′, which are renormalization group invariants. The n_f (n'_f) counts the number of (mirror) quark flavors involved at a given scale μ. Then, we can match $\alpha_s(\mu)$ at the scale $\mu = m_t$ with $n_f = 5$ and $n_f = 6$,

$$\alpha_s^{(5)}(m_t) = \alpha_s^{(6)}(m_t), \tag{3.6}$$

which leads to

$$\Lambda_{(5)} = (m_t)^{2/23}(\Lambda_{(6)})^{21/23}. \tag{3.7}$$

Similarly, matching $\alpha_s(\mu)$ at $\mu = m_b$ and $\mu = m_c$, respectively, we deduce

$$\Lambda_{(4)} = (m_b)^{2/25}(\Lambda_{(5)})^{23/25}, \tag{3.8}$$

$$\Lambda_{(3)} = (m_c)^{2/27}(\Lambda_{(4)})^{25/27}. \tag{3.9}$$

From the above relations, we further arrive at

$$\Lambda_{(3)} = (m_c m_b m_t)^{2/27}(\Lambda_{(6)})^{21/27} \propto v_\phi^{2/9}(\Lambda_{(6)})^{21/27}, \tag{3.10}$$

where we note that the current quark masses for (c, b, t) are generated from the Yukawa interactions with Higgs boson ϕ, and thus are proportional to the Higgs VEV v_ϕ. The nucleon consists of up and down quarks and its mass is dominated by the dynamical mass instead of the current masses of u and d quarks (which are only a few MeV and thus negligible here). So, the nucleon mass should be proportional to the dynamical QCD scale $\Lambda_{(3)}$. Thus, using (3.10) we finally derive

$$m_N \propto v_\phi^{2/9}(\Lambda_{(6)})^{21/27}. \tag{3.11}$$

In parallel, we can infer the relation for mirror nucleon mass,

$$m_{N'} \propto v_{\phi'}^{2/9}(\Lambda'_{(6)})^{21/27}. \tag{3.12}$$

Note that the visible (mirror) sector contains only six (mirror) quark flavors, so the renormalization group invariant $\Lambda_{(6)}$ (or $\Lambda'_{(6)}$) holds for all scales above m_t (or m'_t). At sufficiently high scales $\mu \gg m_t, m'_t \sim v_\phi, v'_\phi$, the renormalization group invariants $\Lambda_{(6)}$ and $\Lambda'_{(6)}$ are determined by the corresponding strong gauge couplings alone. As the mirror symmetry requires $\alpha_s(\mu) = \alpha'_s(\mu)$, it leads to $\Lambda_{(6)} = \Lambda'_{(6)}$. With this we can deduce from (3.11) and (3.12),

$$\frac{m_{N'}}{m_N} = \left(\frac{v_{\phi'}}{v_\phi}\right)^{2/9}. \tag{3.13}$$

Next, we analyze the ratio of visible and mirror baryon numbers, $\mathcal{N}_{\rm B'}/\mathcal{N}_{\rm B}$, as appeared in Eq. (3.3). It is natural and attractive to produce $\mathcal{N}_{\rm B}$ and $\mathcal{N}_{\rm B'}$ from the visible and mirror leptogeneses via neutrino seesaws, respectively. As we will show, due to the mirror parity, the visible and mirror neutrino seesaws are quantitatively connected; especially, they share the same CP phases in addition to the same Yukawa couplings and singlet heavy Majorana mass matrix. This naturally provides a common origin for the visible matter and mirror dark matter via leptogeneses. As we mentioned earlier, we will allow soft breaking of mirror parity in the gauge-singlet sectors which include the heavy singlet Majorana mass terms in the neutrino seesaw [35]. This means that we will allow unequal singlet heavy Majorana mass matrices, $M_N \neq M'_N$, between the visible and mirror seesaws; but we will maintain this soft breaking to be minimal, i.e., both M_N and M'_N still have identical structure (as required by mirror parity) except differing by an overall scaling factor, $M_N \propto M'_N$. Hence, we can write down the seesaw Lagrangian,

$$\begin{aligned}\mathcal{L}_{\rm ss} &= -\bar{L}Y_\ell \phi \ell_R - \bar{L}Y_\nu \tilde{\phi}\mathbb{N} + \tfrac{1}{2}\mathbb{N}^T M_N \hat{C}\mathbb{N} \\ &\quad - \bar{R}'Y'_\ell \phi' \ell'_L - \bar{R}'Y'_\nu \tilde{\phi}'\mathbb{N}' + \tfrac{1}{2}\mathbb{N}'^T M'_N \hat{C}\mathbb{N}' \\ &\quad + \tfrac{1}{2}\mathbb{N}^T \delta m \hat{C}\mathbb{N}' + \text{H.c.} \qquad (3.14a) \\ &= -\overline{\ell_L} M_\ell \ell_R - \overline{\nu_L} m_D \mathbb{N} + \tfrac{1}{2}\mathbb{N}^T M_N \hat{C}\mathbb{N} \\ &\quad - \overline{\ell'_R} M'_\ell \ell'_L - \overline{\nu'_R} m'_D \mathbb{N}' + \tfrac{1}{2}\mathbb{N}'^T M'_N \hat{C}\mathbb{N}' \\ &\quad + \tfrac{1}{2}\mathbb{N}^T \delta m \hat{C}\mathbb{N}' + \text{H.c.} + (\text{interactions}), \qquad (3.14b)\end{aligned}$$

where L denotes three left-handed neutrino-lepton weak doublets, $\ell = (e, \mu, \tau)^T$ contains charged leptons, $\nu = (\nu_e, \nu_\mu, \nu_\tau)^T$ is for the light flavor neutrinos, and $\mathbb{N} = (N_1, N_2, N_3)^T$ represents two heavy right-handed singlet neutrinos for the visible sector, while R', $\ell' = (e', \mu', \tau')^T$, $\nu' = (\nu'_e, \nu'_\mu, \nu'_\tau)^T$, and $\mathbb{N}' = (N'_1, N'_2, N'_3)^T$ are the corresponding fields in the mirror sector. In (3.14),

we have used $\tilde{\phi}$ ($\tilde{\phi}'$) to denote the charge-conjugation of Higgs doublet ϕ (mirror Higgs doublet ϕ'), and $\hat{C} = i\gamma^2\gamma^0$ is the charge-conjugation operator for spinors. Also, the notations for singlet heavy Majorana neutrinos $\mathbb{N}$ and $\mathbb{N}'$ are connected to that in (2.1) via $\mathbb{N} \sim \nu_R$ and $\mathbb{N}' \sim \nu'_L$, where $\mathbb{N}$ and $\mathbb{N}'$ are Majorana spinors, so we have $\mathbb{N} = \mathbb{N}^c$ and $\mathbb{N}' = \mathbb{N}'^c$.

Imposing the mirror symmetry P on the interaction Lagrangian in (3.14a) of neutrino seesaw and allowing the minimal soft P-breaking for the heavy singlet Majorana mass terms in (3.14a), we deduce the following relations between the visible and mirror sectors:

$$Y_\ell = Y'_\ell, \qquad Y_\nu = Y'_\nu, \qquad M_N = r_N M'_N, \tag{3.15}$$

where the ratio $r_N \equiv M'_N/M_N \neq 1$ characterizes the minimal soft P-breaking and its value will be determined later by generating the desired dark matter density, $\Omega_{\rm DM} \simeq 5\Omega_{\rm M}$. The mass eigenvalues of M_N and M'_N will be denoted as M_j and M'_j, respectively. Thus we also have $M_j/M'_j = r_N$. Since the Dirac mass matrices $m_D = Y_\nu v_\phi$ and $m'_D = Y'_\nu v_{\phi'}$, we have

$$\frac{m'_D}{m_D} = \frac{v_{\phi'}}{v_\phi}. \tag{3.16}$$

Since the mixing mass term δm between $\mathbb{N} - \mathbb{N}'$ in (3.14) will lead to mixings between light visible and mirror neutrinos after the heavy singlet neutrinos $\mathbb{N}$ and $\mathbb{N}'$ are integrated out, this term has to be very small due to the tight constraints for sterile neutrinos. So we have $\delta m \ll | M_R - M'_R |$ and thus for the present analysis it is safe to neglect δm. This means that we have separate seesaw mass formulas for the light visible and mirror neutrinos,

$$M_\nu \simeq m_D M_N^{-1} m_D^T, \tag{3.17a}$$

$$M'_\nu \simeq m'_D M'^{-1}_N m'^T_D = \frac{v^2_{\phi'}}{v^2_\phi} r_N M_\nu, \tag{3.17b}$$

where in the second equation we have used the mirror symmetric relations (3.15) and (3.16). These show that the visible and mirror neutrino sectors must share the same CP violation phase(s) as well as the same flavor mixing structure.

In the visible sector, the baryon number density $\mathcal{N}_B$ and the amount of $B - L$ asymmetry $\mathcal{N}_{B-L}$, as defined in a portion of comoving volume containing one photon at the onset of leptogenesis, are given by [9]

$$\mathcal{N}_B = \xi \mathcal{N}_{B-L} = \frac{3}{4}\xi \kappa_f \epsilon_1, \tag{3.18}$$

where the parameter $\xi = 28/79$ is the fraction of $B - L$ asymmetry converted from $\mathcal{N}_{B-L}$ into a net baryon number $\mathcal{N}_B$ by sphaleron processes, and is determined by the number of fermion generations and Higgs doublets in the SM [36]. The factor κ_f in (3.18) measures the efficiency of out-of-equilibrium N_1-decays, and ϵ_1 characterizes the CP asymmetry produced by the decays of the lighter singlet neutrino N_1 at the scale of M_1. In parallel, for the mirror sector we have

$$\mathcal{N}'_B = \xi' \mathcal{N}'_{B-L} = \tfrac{3}{4}\xi' \kappa'_f \epsilon'_1, \tag{3.19}$$

where $\xi' = \xi = 28/79$, since the mirror sector has the same number of fermion generations and Higgs doublets as the visible sector. The P-odd singlet scalar χ is real and thus has zero chemical potential. Also, in the Higgs potential (2.8), all the mixing terms among ϕ, ϕ', and χ have vanishing chemical potential. So they do not affect the conversion efficiencies ξ and ξ' in both visible and mirror sectors, and we have $\xi = \xi'$.

The efficiency factor κ_f in (3.18) can be solved from the Boltzmann equations [37],

$$\frac{d\mathcal{N}_{N_1}}{dz} = -(D + S)(\mathcal{N}_{N_1} - \mathcal{N}^{\rm eq}_{N_1}), \tag{3.20a}$$

$$\frac{d\mathcal{N}_{B-L}}{dz} = -\epsilon_1 D(\mathcal{N}_{N_1} - \mathcal{N}^{\rm eq}_{N_1}) - W\mathcal{N}_{B-L}, \tag{3.20b}$$

where $z = M_1/T$, and $(D, S, W) = (\Gamma_D, \Gamma_S, \Gamma_W)/(Hz)$ are dimensionless functions of z. The Hubble expansion rate H is given by, $H \simeq (8\pi^3 g_*/90)^{1/2}(M_1^2/M_{\rm P})z^{-2}$, where $M_{\rm P} \simeq 1.22 \times 10^{19}$ GeV equals the Planck mass, and g_* represents the relativistic degrees of freedom at the temperature T. The rate Γ_D denotes the decays and inverse decays of N_1, Γ_S accounts for N_1 scattering rate, and Γ_W is the washout rate including contributions from the inverse decays and the $\Delta L = 1, 2$ processes, where the contribution of $\Delta L = 2$ processes is denoted by $\Delta\Gamma_W \equiv (Hz)\Delta W$. It is found [37] that the dimensionless functions (D, S, W, ΔW) have the following simple scalings:

$$D, S, W - \Delta W \propto \frac{M_{\rm P}\tilde{m}_1}{v^2_\phi}, \qquad \Delta W \propto \frac{M_{\rm P} M_1 \bar{m}^2}{v^4_\phi}, \tag{3.21}$$

where $\tilde{m}_1$ is the effective light neutrino mass,

$$\tilde{m}_1 \equiv \frac{(\tilde{m}^\dagger_D \tilde{m}_D)_{11}}{M_1}, \tag{3.22}$$

and $\tilde{m}_D \equiv m_D V_R$, with V_R being the unitary rotation matrix which diagonalizes M_R. In the last relation of (3.21), the light neutrino mass parameter $\bar{m}$ is given by the trace $\bar{m} = [{\rm tr}(M^\dagger_\nu M_\nu)]^{1/2} = \sqrt{m_1^2 + m_2^2 + m_3^2}$. Inspecting (3.21), (3.22), and (3.17a), we note that the functions (D, S, W, ΔW) do not actually depend on the Higgs VEV v_ϕ, but depend on relevant products of Yukawa couplings and the heavy singlet neutrino mass M_1 as well as the Planck mass $M_{\rm P}$. We can see this explicitly by examining the analytical solution [37] of the Boltzmann equations (3.20),

$$\kappa_f \simeq \frac{2}{z_B(K)K}\left[1-\exp\left(-\frac{1}{2}z_B(K)K\right)\right], \tag{3.23a}$$

$$z_B(K) \simeq 1+\frac{1}{2}\ln\left[1+\frac{\pi K^2}{1024}\left(\ln\frac{3125\pi K^2}{1024}\right)^5\right], \tag{3.23b}$$

which agrees with the exact numerical solution very well. This shows that the efficiency factor κ_f depends only the parameter K,

$$K=\frac{\Gamma_D(z=\infty)}{H(z=1)}=\frac{\tilde{m}_1}{m_*}\propto\frac{1}{M_1}, \tag{3.24a}$$

$$m_*=\frac{16\pi^{5/2}\sqrt{g_*}}{3\sqrt{5}}\frac{v_\phi^2}{M_{\rm P}}\simeq 1.5\times10^{-3}\ \text{eV}, \tag{3.24b}$$

where the VEV $v_\phi \simeq 174$ GeV is responsible for the electroweak symmetry breaking (cf. Sec. IV). At the temperature $T\sim M_1$, we note that the effective degrees of freedom $g_*=O(200)$ contain 106.75 from SM particles and $\frac{7}{4}$ from Majorana neutrino N_1, and in addition, the mirror partners contribute another 106.75 to g_* and the real scalar χ contributes 1. So we have $g_*=216.25$ in total. (Here we do not count on the lightest mirror singlet neutrino N_1' because its mass is much larger than N_1 [cf. (3.35) below] and already decays at a higher temperature.) Inspecting (3.22) and (3.24), we note that $K\propto M_1^{-1}$, but has no dependence on the Higgs VEV v_ϕ because both $\tilde{m}_1$ and m_* are proportional to v_ϕ^2.

For practical applications, it is more convenient to use the fitting formula for the efficiency factor κ_f in the power-law form under $\tilde{m}_1 > m_*$ [37],

$$\kappa_f=(2\pm1)\times10^{-2}\left(\frac{0.01\ \text{eV}}{\tilde{m}_1}\right)^{1.1\pm0.1}\propto M_1^{(1.1\pm0.1)}, \tag{3.25}$$

where the effective light neutrino mass $\tilde{m}_1$ is defined in (3.22) and we have extracted the scaling behavior $\kappa_f\propto M_1^{(1.1\pm0.1)}$. The formula (3.25) is found to be in good agreement with the exact numerical solution [37]. We expect that, without accidental cancellation, effective mass $\tilde{m}_1$ should be the typical mass scale of light neutrinos, i.e., $\tilde{m}_1=O(10^{-1}$–$10^{-2})$ eV. For natural Yukawa couplings $Y_\nu\le O(1)$, one can infer [37], $m_1\le\bar{m}_1\le m_3$ or $m_3\le\bar{m}_1\le m_1$. As will be shown in Sec. III [cf. Eq. (3.43a)], for our explicit seesaw realizations, we can deduce $\tilde{m}_1\sim\sqrt{\Delta m_{13}^2}=O(10^{-1}$–$10^{-2})$ eV, where Δm_{13}^2 is the atmospheric mass-squared difference as measured by the oscillation experiments [38]. For computing the ratio of the two efficiency factors κ_f and κ_f' in the visible and mirror sectors, we see that the overall coefficient on the RHS of (3.25) is irrelevant; only the scaling behaviors, $\kappa_f\propto M_1^{(1.1\pm0.1)}$ and $\kappa_f'\propto M_1'^{(1.1\pm0.1)}$, will matter. So, we can deduce the ratio

$$\frac{\kappa_f'}{\kappa_f}=\left(\frac{M_1'}{M_1}\right)^{1.1\pm0.1}=\left(\frac{1}{r_N}\right)^{1.1\pm0.1}, \tag{3.26}$$

which depends on the mass ratio r_N of the visible/mirror heavy singlet neutrinos, and does not equal 1 due to the soft breaking of mirror parity in the singlet sector, $M_1\neq M_1'$, as in (3.15).

The CP asymmetry parameter ϵ_1 can be expressed as

$$\begin{aligned}\epsilon_1&=\frac{\Gamma[N_1\to\ell H]-\Gamma[N_1\to\bar{\ell}H^*]}{\Gamma[N_1\to\ell H]+\Gamma[N_1\to\bar{\ell}H^*]}\\&=\frac{1}{4\pi v_\phi^2}F\left(\frac{M_2}{M_1}\right)\frac{\Im\mathrm{m}\{[(\tilde{m}_D^\dagger\tilde{m}_D)_{12}]^2\}}{(\tilde{m}_D^\dagger\tilde{m}_D)_{11}},\end{aligned} \tag{3.27}$$

where the v_ϕ factors all cancel out on the right-hand-side, and for the SM the function $F(x)$ takes the following form:

$$\begin{aligned}F(x)&\equiv x\left[1-(1+x^2)\ln\frac{1+x^2}{x^2}+\frac{1}{1-x^2}\right]\\&=-\frac{3}{2x}+\mathcal{O}\left(\frac{1}{x^3}\right),\qquad(\text{for } x\gg1).\end{aligned} \tag{3.28}$$

In parallel, for the mirror CP-asymmetry parameter ϵ_1', we have

$$\begin{aligned}\epsilon_1'&=\frac{\Gamma[N_1'\to\ell_R'H']-\Gamma[N_1'\to\bar{\ell}_R'H'^*]}{\Gamma[N_1'\to\ell_R'H']+\Gamma[N_1'\to\bar{\ell}_R'H'^*]}\\&=\frac{1}{4\pi v_{\phi'}^2}F\left(\frac{M_2'}{M_1'}\right)\frac{\Im\mathrm{m}\{[(\tilde{m}_D'^\dagger\tilde{m}_D')_{12}]^2\}}{(\tilde{m}_D'^\dagger\tilde{m}_D')_{11}}.\end{aligned} \tag{3.29}$$

Because of the soft-breaking relation $M_N\propto M_N'$ in (3.15), we have equal mass ratios $M_2/M_1=M_2'/M_1'$. Using the mirror symmetry requirements (3.15) and (3.16), and noting that the VEV factors all drop off in (3.27) and (3.29), we deduce

$$\epsilon_1'=\epsilon_1. \tag{3.30}$$

Hence, the difference between $\mathcal{N}_B$ and $\mathcal{N}_B'$ actually arises from the parameters κ_f and κ_f' as in (3.26). Now, from (3.18), (3.19), and (3.26), we can deduce the ratio of visible and mirror baryon asymmetries,

$$\frac{\mathcal{N}_B'}{\mathcal{N}_B}=\frac{\xi'\kappa_f'\epsilon_1'}{\xi\kappa_f\epsilon_1}=\frac{\kappa_f'}{\kappa_f}=\left(\frac{M_1'}{M_1}\right)^{1.1\pm0.1}. \tag{3.31}$$

With (3.3), (3.13), and (3.31), we finally arrive at

$$\frac{\Omega_{\rm DM}}{\Omega_{\rm M}}=\frac{\Omega_{B'}}{\Omega_B}=\frac{\mathcal{N}_B'}{\mathcal{N}_B}\frac{m_N'}{m_N}=\left(\frac{M_1'}{M_1}\right)^{(1.1\pm0.1)}\left(\frac{v_{\phi'}}{v_\phi}\right)^{2/9}. \tag{3.32}$$

Thus, to realize the astrophysical observation of $\Omega_{\rm DM}/\Omega_{\rm M}=5.0\pm0.74$ as inferred from (3.1) and (3.2) [34], we deduce a constraint on the ratio between the visible and mirror heavy singlet neutrino masses,

$$\frac{M_1'}{M_1} = \left(\frac{\Omega_{\rm DM}}{\Omega_{\rm M}}\right)^{1/\varrho}\left(\frac{v_\phi}{v_{\phi'}}\right)^{2/(9\varrho)}, \tag{3.33}$$

where $\varrho \equiv 1.1 \pm 0.1$. As we will show in (3.51) of Sec. III, the big-bang nucleosynthesis (BBN) will put nontrivial constraint on the VEV ratio, $v_{\phi'}/v_\phi < 0.70$. Combining with the naturalness condition (3.26), we have

$$0.1 < \frac{v_{\phi'}}{v_\phi} < 0.7. \tag{3.34}$$

Taking the ratio $v_{\phi'}/v_\phi = (0.1, 0.5, 0.7)$, we evaluate the VEV factor in (3.33) with $\varrho = 1.1$ and find, $(v_\phi/v_{\phi'})^{2/(9\varrho)} = (1.6, 1.2, 1.1)$, respectively, which is rather insensitive to $v_{\phi'}/v_\phi$. So, in the numerical analyses of Secs. IV, we will set a sample value of $v_{\phi'}/v_\phi = \frac{1}{2}$. With this model input and $\varrho = 1.1$, we derive the constraint for the mass ratio of heavy singlet neutrinos, $r_N \equiv M_1/M_1'$,

$$0.18 < r_N < 0.23, \tag{3.35}$$

with a central value $r_N = 0.2$, where we have imposed the 2σ astrophysical limit on the ratio of dark matter over matter densities, $4.26 < \Omega_{\rm DM}/\Omega_{\rm M} < 5.74$.

B. Explicit seesaw realizations of visible/dark matter genesis

In this subsection, we will extend two of our seesaw constructions [39,40] to the present visible and mirror neutrino sectors, where the $\mu - \tau$ and CP symmetry breakings naturally arise from a common origin. With these, we show how the common origin of visible and dark matter geneses are explicitly realized in the seesaw formalism. Also, as given in Eq. (3.25), we see that κ_f (or similarly κ_f') depends on the mass parameters $\tilde{m}_1$ (or $\tilde{m}_1'$). We expect that $\tilde{m}_1$ should be the typical mass scale of light neutrinos, around $\tilde{m}_1 = O(10^{-1}$–$10^{-2})$ eV. With the seesaw formalisms [39,40], we will derive $\tilde{m}_1$ and $\tilde{m}_1'$ explicitly, which also justify the conditions $\tilde{m}_1 > m_*$ and $\tilde{m}_1' > m_*'$, for the application of κ_f formula (3.25) and its extension to κ_f'.

The $\mu - \tau$ symmetry is a $\mathbb{Z}_2$ invariance of the light neutrino mass matrix M_ν under the exchange $\nu_\mu \leftrightarrow \nu_\tau$. The $\mu - \tau$ symmetric limit predicts a unique pattern for atmospheric and reactor neutrino mixing angles, $\theta_{23} = 45^\circ$ and $\theta_{13} = 0^\circ$. This is strongly supported by the existing neutrino oscillation data as a good zeroth-order symmetry, because both deviations $\theta_{23} - 45^\circ$ and $\theta_{13} - 0^\circ$ are constrained to be generically small, $-7.5^\circ < \theta_{23} - 45^\circ < 2.9^\circ$ and $5.1^\circ < \theta_{13} - 0^\circ < 10^\circ$ at 90% C.L. [38], which are all within a 10° range. A vanishing θ_{13} also enforces the absence of Dirac CP violation, so under the attractive conjecture that all CP violations arise from a common origin in the neutrino seesaw, it is deduced that all CP violations share a common origin with $\mu - \tau$ breaking [39,40]. We also note that under $\mu - \tau$ symmetry, the singlet heavy Majorana neutrinos can either transform simultaneously or act as $\mu - \tau$ singlets since the low energy oscillation data only measure the mixings encoded in the light neutrino mass matrix. In the first case, we found that the common origin of $\mu - \tau$ and CP violations can be formulated as the unique soft breaking via dimension-3 mass term of heavy singlet Majorana neutrinos [39]; while in the second case (called the $\mu - \tau$ blind seesaw), we found that this common breaking can be uniquely formulated in the Dirac mass term from Yukawa interactions [40].

In the following, we will extend these two constructions to the present mirror model where the mirror symmetry enforces the visible and mirror neutrino seesaws to share the common origin of $\mu - \tau$ and CP breaking, and thus the common origin for visible and mirror leptogeneses with the same CP phase in the N_1 and N_1' decays. For simplicity, we consider the minimal seesaw with two singlet heavy Majorana neutrinos, in the visible and mirror sectors, respectively. This ensures one of the light neutrinos to be massless under seesaw and thus predicts the hierarchical mass spectrum for light neutrinos (with normal or inverted mass ordering). This is always a good approximation when the third singlet Majorana neutrino is much heavier than the other two and thus decoupled from the seesaw Lagrangian. Extensions to general three-neutrino seesaw were also considered in [39,40], where a massless light neutrino is still predicted even after including the common $\mu - \tau$ and CP breaking.

1. Visible/mirror seesaws with common soft $\mu - \tau$ and CP breaking

For the soft $\mu - \tau$ and CP breaking from a common origin in the neutrino seesaw, we find that they uniquely arise from the dimension-3 mass term of singlet heavy Majorana neutrinos. For the visible neutrino seesaw, we have the Dirac and Majorana mass matrices including the common soft $\mu - \tau$ and CP breaking [39],

$$m_D = \begin{pmatrix} a & a \\ b & c \\ c & b \end{pmatrix}, \quad M_N = \begin{pmatrix} M_{22} & M_{23} \\ M_{23} & M_{22}(1 - \zeta e^{i\omega}) \end{pmatrix}, \tag{3.36}$$

where the small breaking is characterized by the module $0 < \zeta < 1$ and CP angle $\omega \in [0, 2\pi)$. Accordingly, for the mirror neutrino seesaw we have

$$m_D' = \frac{v_{\phi'}}{v_\phi} m_D, \qquad M_N' = \frac{1}{r_N} M_N. \tag{3.37}$$

Here the minimal soft P-breaking is realized by the overall ratio $r_N \approx 0.2 \neq 1$, and the proportionality of $M_N' \propto M_N$ ensures the same structure of M_N and M_N', i.e., the visible and mirror sectors share the common origin of CP violation, which will thus serve as the common genesis

for matter and dark matter in the two sectors. The mass spectrum of light neutrinos falls into the normal mass ordering (NMO) pattern ($0 = m_1 < m_2 \ll m_3$), where the zero mass eigenvalue $m_1 = 0$ was found to persist even in the generalized three-neutrino seesaw with common soft $\mu - \tau$ and CP breaking [39]. From systematical derivations [39], we have

$$\tilde{m}_1 \equiv \frac{(\tilde{m}_D^\dagger \tilde{m}_D)_{11}}{M_1} \simeq \frac{(b-c)^2}{M_1} \simeq \chi_1 m_3 = \chi_1 \sqrt{\Delta m^2_{13}}, \quad (3.38)$$

where the third light neutrino mass $m_3 = \sqrt{\Delta m^2_{13}}$ for the NMO spectrum, and the mass-squared difference $\Delta m^2_{13} \equiv |m_3^2 - (m_2^2 + m_1^2)/2|$ is measured to be $2.06 \times 10^{-3} < \Delta m^2_{31} < 2.67 \times 10^{-3}$ eV^2 at 3σ level, with the central value $\sqrt{\Delta m^2_{31}} = 0.048$ eV [38]. The coefficient $\chi_1 = \chi(M_1, M_Z)$ in (3.38) is a renormalization group running factor which evolves m_3 from weak scale M_Z up to the leptogenesis scale M_1, and is found to be about 1.3–1.4 for $M_1 = 10^{13}$–10^{16} GeV [39]. So we can estimate, $\tilde{m}_1 \simeq 0.06$–0.07 eV $> m_*$, where $m_* \simeq 1.5 \times 10^{-3}$ eV is given in (3.24b).

For the mirror neutrino seesaw, we can deduce from (3.37) and (3.38),

$$\tilde{m}'_1 \equiv \frac{(\tilde{m}'^\dagger_D \tilde{m}'_D)_{11}}{M'_1} = \frac{v^2_{\phi'}}{v^2_\phi} r_N \tilde{m}_1. \quad (3.39)$$

As mentioned earlier, from the BBN constraint (Sec. III) and the naturalness consideration, we have $v_{\phi'}/v_\phi \approx \frac{1}{2}$; while with the density ratio of dark matter over matter, we inferred from (3.35), $r_N \approx 0.2$. So we can estimate $\tilde{m}'_1 \approx \tilde{m}_1/20 \simeq (3$–$3.5) \times 10^{-3}$ eV $> m'_*$, since m'_* is given by

$$m'_* = \frac{16\pi^{(5/2)}\sqrt{g'_*}}{3\sqrt{5}} \frac{v^2_{\phi'}}{M_{\rm P}} \simeq 3.8 \times 10^{-4} \text{ eV}, \quad (3.40)$$

where we count $g'_* = 219.75 = O(200)$ at the temperature $T = T' \sim M'_1$, which contains 106.75×2 from the SM degrees of freedom plus their mirror partners, and $\frac{7}{4} \times 3$ for N'_1 and (N_1, N_2), as well as another 1 by the real scalar χ.

2. Visible/mirror $\mu - \tau$ blind seesaws with common $\mu - \tau$ and CP breaking

For the $\mu - \tau$ blind seesaw, the heavy Majorana neutrinos are $\mu - \tau$ singlets, so we can always start with their mass eigenbasis under which M_N and M'_N are diagonal. Thus the Dirac mass terms m_D and m'_D are the unique place for common $\mu - \tau$ and CP breaking [40],

$$m_D = \begin{pmatrix} \bar{a} & \bar{a}' \\ \bar{b} & \bar{c}(1-\zeta') \\ \bar{b} & \bar{c}(1-\zeta e^{i\omega}) \end{pmatrix}, \quad M_N = \begin{pmatrix} M_1 & 0 \\ 0 & M_2 \end{pmatrix}, \quad (3.41a)$$

for the visible neutrino sector, and

$$m'_D = \frac{v_{\phi'}}{v_\phi} m_D, \qquad M'_N = \frac{1}{r_N} M_N, \quad (3.41b)$$

for the mirror neutrino sector, where $0 < \zeta < 1$, $|\zeta'| < 1$, and $\omega \in [0, 2\pi)$ parametrize the $\mu - \tau$ and CP breaking. Hence, it is the proportionality $m_D \propto m'_D$ that ensures the visible and mirror sectors to share the common origin of CP violation, which will then serve as the common genesis for matter and dark matter in the two sectors.

From systematical analysis [40], we see that the light neutrino mass spectrum falls into the inverted mass ordering (IMO) pattern ($m_2 \gtrsim m_1 \gg m_3 = 0$), where we found that the zero mass eigenvalue $m_3 = 0$ persists up to the next-to-leading order even in the generalized three-neutrino seesaw with common $\mu - \tau$ and CP breaking. Then we deduce

$$\tilde{m}_1 \equiv \frac{(\tilde{m}_D^\dagger \tilde{m}_D)_{11}}{M_1} \simeq \chi_1 m_1 \simeq \chi_1 \sqrt{\Delta m^2_{13}}, \quad (3.42a)$$

for the visible seesaw as in [40], and

$$\tilde{m}'_1 \equiv \frac{(\tilde{m}'^\dagger_D \tilde{m}'_D)_{11}}{M'_1} = \frac{v^2_{\phi'}}{v^2_\phi} r_N \tilde{m}_1, \quad (3.42b)$$

for the mirror seesaw.

Comparing (3.42a) and (3.42b) in the $\mu - \tau$ blind seesaw with (3.38) and (3.39) in the soft-breaking seesaw, we can deduce, for both cases,

$$\tilde{m}_1 \simeq \chi_1 \sqrt{\Delta m^2_{13}} \simeq 0.06 - 0.07 \text{ eV} > m_*, \quad (3.43a)$$

$$\tilde{m}'_1 \simeq \frac{v^2_{\phi'}}{v^2_\phi} r_N \tilde{m}_1 = (3 - 3.5) \times 10^{-3} \text{ eV} > m'_*, \quad (3.43b)$$

where we take the ratios $v_{\phi'}/v_\phi \approx \frac{1}{2}$ and $r_N \approx 0.2$, as explained above.

C. Analysis of the BBN constraint

Before concluding this section, we discuss the possible constraint from big-bang nucleosynthesis on the mirror sector. The observed light element abundances in the Universe agree well with the predictions of BBN in the SM of particle physics. This means that at the temperature $T \sim 1$ MeV, the number of effective degrees of freedom should be $g_* = 10.75$ as contributed by photons, electrons, and three species of neutrinos. Considering the mirror model, we have additional contributions from mirror photons, mirror electrons, and mirror neutrinos to g_*. So the total number of degrees of freedom becomes as $\hat{g}_*$,

$$\hat{g}_* = g_* \left[1 + \left(\frac{T'}{T} \right)^4 \right], \quad (3.44)$$

where T (T') is the temperature of visible (mirror) sector. The deviation of $\hat{g}_*$ from g_* is normally parametrized in

terms of the effective number of extra neutrino species ΔN_ν via $\Delta g_* = \hat{g}_* - g_* = 1.75\Delta N_\nu$. So we have

$$\Delta N_\nu \simeq 6.14\left(\frac{T'}{T}\right)^4. \tag{3.45}$$

But the current BBN analysis gives [41] $N_\nu = 3.80^{+0.80}_{-0.70}$ at 2σ level, for the neutron lifetime being $878.5 \pm 0.8s$. So this puts a 2σ upper limit, $\Delta N_\nu < 1.50$, and thus imposes the constraint on the mirror temperature T' in the BBN epoch,

$$T' < 0.70T, \tag{3.46}$$

where the coefficient is proportional to $(\Delta N_\nu)^{1/4}$, with only a mild dependence on ΔN_ν. In the literature [42,43], it was assumed that after inflation the reheating temperatures in the two sectors are different such that the condition (3.46) will be obeyed during BBN. But it is not the case for the current construction due to the mixed Higgs interactions $|\phi|^2|\phi'|^2$, $\chi|\phi|^2$, and $\chi|\phi'|^2$ in (2.8a), which will bring the two sectors into thermal equilibrium before BBN starts (even though the kinetic mixing between photons and mirror photons in (2.6) may be negligible).

Our model realizes (3.46) in a different way. For the above reason, we simply have the equal temperatures $T = T'$ for the two sectors after inflation and then at the leptogenesis scale M_N and M'_N. We observe that the desired temperature difference in (3.46) can be produced through the visible and mirror electroweak phase transitions at the scales $\sim(v_\chi, v_\phi, v_{\phi'}) = O(100\ \text{GeV})$. For simplicity of illustration, let us first write down the one-loop effective potential for scalar field χ alone at temperature T. Defining the thermal average $\langle\chi\rangle = \chi_c$, we have

$$\begin{aligned} V(\chi_c) = &\left[-\frac{1}{2}\mu_\chi^2\chi_c^2 + \frac{1}{4}\lambda_\chi\chi_c^4\right] \\ &+ \left[\frac{\lambda_\chi}{6}T^2\chi_c^2 - \frac{\pi^2}{90}\left(N_B + \frac{7}{8}N_F\right)T^4\right] \\ &+ \frac{3\lambda_\chi^2}{128\pi^2}\chi_c^4\left(\ln\frac{\chi_c^2}{M^2} - \frac{25}{6}\right), \end{aligned} \tag{3.47}$$

where on the RHS inside the second brackets is the finite temperature correction and the last line gives the Coleman-Weinberg term. In the effective potential above, N_B (N_F) denotes the number of bosonic (fermionic) degrees of freedom. At finite temperature, the Higgs mass term receives a correction from the thermal fluctuation and becomes

$$m_\chi^2(T) = -\mu_\chi^2 + \frac{\lambda_\chi}{3}T^2. \tag{3.48}$$

Near the critical temperature $T_c = \mu_\chi\sqrt{\frac{3}{\lambda_\chi}}$, we have the scalar mass $m_\chi^2 \simeq 0$, so the effective potential takes the form

$$\begin{aligned} V(\chi_c) = &\frac{3\lambda_\chi^2}{128\pi^2}\chi_c^4\left(\ln\frac{\chi_c^2}{M^2} - \frac{25}{6}\right) + \frac{1}{4}\lambda_\chi\chi_c^4 \\ &- \frac{\pi^2}{90}\left(N_B + \frac{7}{8}N_F\right)T^4. \end{aligned} \tag{3.49}$$

A kind of scalar potential similar to (3.49) was also used to generate the electroweak scale inflation in Ref. [44] for a singlet inflaton field at the weak scale. It was found that this can result in about 30 e-foldings at the weak scale. We do not need such huge expansion at this stage since we have the conventional high-scale inflation in our scheme. But from this we see that it is easy for the electroweak phase transition of a Higgs field to cause a small expansion just about $1 \sim 2$ e-foldings [45], starting from the temperature [46] $T = T' \sim \max(v_\chi, v_\phi, v_{\phi'})$. And then T rolls down together with T'. After these three Higgs bosons roll into the potential minimum at lower temperature, the reheatings [47] from the electroweak vacuum energies start. The vacuum energy density in (2.11b) takes the forms of v_χ^4, $v_\chi^2 v_\phi^2$, v_ϕ^4, $v_\chi^2 v_{\phi'}^2$, $v_\phi^2 v_{\phi'}^2$, and $v_{\phi'}^4$. Under the explicit constructions in Sec. IV, we will always have the mass eigenstate Higgs $\hat{\chi}$ and $\hat{\phi}$ dominantly decay into the visible SM particles, and the mirror Higgs $\hat{\phi}'$ mainly decay into mirror particles. So the reheatings of vacuum energies associated with $\hat{\chi}$ and $\hat{\phi}$ will raise the temperature of the visible sector back to $T \sim \max(v_\chi, v_\phi)$, and the reheating with $\hat{\phi}'$ raises the temperature of the mirror sector back to $T' \sim v_{\phi'}$. So, the visible and mirror reheatings end up with a temperature relation

$$\frac{T'}{T} \sim \frac{v_{\phi'}}{\max(v_\chi, v_\phi)} \sim \frac{v_{\phi'}}{v_\chi}, \frac{v_{\phi'}}{v_\phi}. \tag{3.50}$$

After reheatings, the temperature difference (3.50) remains along the expansion of the Universe till the BBN epoch at $T \sim 1$ MeV. Combining the BBN condition (3.46) with (3.50), we find the VEV ratio is subject to the constraint

$$\frac{v_{\phi'}}{v_\chi}, \frac{v_{\phi'}}{v_\phi} < 0.7. \tag{3.51}$$

For sufficient reheatings with 100 percent conversion of the vacuum energies into radiations, we need Higgs oscillations to decay rapidly, with $\Gamma_S \gtrsim H$ [47], where Γ_S denotes the decay width of a given scalar S, and H is the Hubble expansion rate at the electroweak phase transition as determined by

$$H \simeq \sqrt{\frac{8\pi\langle V(S)\rangle}{3M_{\text{Pl}}^2}} \sim \sqrt{\frac{8\pi}{3}}\frac{v_S^2}{M_{\text{Pl}}} \sim 10^{-15}\ \text{GeV}, \tag{3.52}$$

where $\langle V(S)\rangle \sim v_S^4$ is the typical vacuum potential of a scalar $S(= \chi, \phi, \phi')$ with its VEV $v_S = O(100)$ GeV at the weak scale. For our model, the typical decay width of S is found to be $\Gamma_S = O(10^{-5} - 1)$ GeV (cf. Sec. VI), so

from (3.52) we have $\Gamma_S \gg H$, showing that the electroweak vacuum energies are fully converted to radiations. Since all Higgs bosons decay away by the end of electroweak vacuum reheating, the mixed interactions like $|\phi|^2|\phi'|^2$ could only occur via virtual processes and are much suppressed. So the thermal contact between the visible and mirror sectors is negligible, and thus the temperature difference (3.50) is retained. There could be potential mixing between visible and mirror photons as in (2.6), but we find that in our model their mixing parameter is constrained down to $\epsilon < 3.4 \times 10^{-5}$ due to the orthopositronium bound [cf. (4.26) in Sec. IV] and $\epsilon \leq 10^{-8}$ due to the direct dark matter search limit of TEXONO [cf. Fig. 6(b) in Sec. VI], so it will not affect the temperature difference (3.50).

IV. HIGGS MASSES, COUPLINGS, AND LOW-ENERGY CONSTRAINTS

In this section we present realistic numerical samples of our model-predictions that can be tested at colliders. For the successful matter and dark matter genesis (Secs. III) and the realization of BBN (Sec. III), we have derived constraints on the mass ratio of heavy singlet neutrinos and the ratio of Higgs boson VEVs between the visible and mirror sectors, as in (3.35) and (3.51). With the vacuum minimization conditions for spontaneous mirror parity violation and electroweak symmetry breaking in Sec. II, we first analyze the viable parameter space. Then, we will present three numerical samples under (3.51), and derive the corresponding Higgs mass spectrum and couplings. Finally, we analyze the constraints from the direct Higgs search and indirect electroweak precision data.

A. Analytical constraints on the parameter space

There are seven free parameters in the Higgs potential (2.8a), including two masses and five couplings. The soft-breaking term (2.8b) contains an extra coefficient β_χ. But we need to impose the following nontrivial physical constraints, which will largely reduce the number of input parameters of our Higgs potential. These constraints are: (i) the VEV of ϕ must generate the right amount of electroweak symmetry breaking in the visible sector, i.e., we have $v_\phi = (2\sqrt{2}G_F)^{1/2} \simeq 174$ GeV. (ii) For successful mirror dark matter genesis and realization of BBN, the ratio of the Higgs VEVs should obey the condition (3.51). (iii) Both the mixings between $\phi' - \chi$ and between $\phi - \phi'$ should be small, so that decays of the mass eigenstate of ϕ or χ into mirror fermions and gauge bosons are negligible. This is to ensure that during the reheating of electroweak phase transition the decays of the mass eigenstates of ϕ and χ will mainly heat up the temperature T of the visible sector, but without affecting the temperature T' of the mirror sector (cf. Sec. III). This last constraint also implies that the mass eigenstate of mirror Higgs ϕ' mainly decouples from the visible sector. These are unique features of our construction and differ from all previous mirror models in the literature.

We note that among all seven parameters in the Higgs potential (2.8a), we have three with mass-dimension-1, $(\mu_\phi, \mu_\chi, \beta_{\chi\phi})$, and the remaining four are dimensionless couplings. The second-order derivative of the vacuum potential (2.11b) at the minimum should be positive. This means that the Higgs mass matrix (2.21) should be positive-definite, so we can infer the following conditions:

$$\lambda_\phi^+ > 0, \qquad \lambda_\phi^- > 0, \tag{4.1a}$$

$$2\lambda_\phi^+\lambda_\phi^-[-\mu_\chi^2 + 3\lambda_\chi v_\chi^2 + \lambda_{\chi\phi}(v_\phi^2 + v_{\phi'}^2)] - \lambda_\phi^+\beta_{\chi\phi}^2 - \lambda_\phi^-\lambda_{\chi\phi}^2 v_\chi^2 > 0. \tag{4.1b}$$

Furthermore, whole potential (2.11b) should be bounded from below. This is determined by the coefficients of the quartic terms. Let us rewrite the quartic interactions of (2.8a) in terms of quadratical form $\Omega^T\mathcal{C}\Omega$ where $\Omega = (|\phi|^2, |\phi'|^2, \chi^2)$ and $\mathcal{C}$ is a 3×3 matrix including the relevant quartic Higgs couplings. So, requiring the matrix $\mathcal{C}$ to be positive-definite, we deduce a new condition in addition to (4.1a),

$$\lambda_\phi^+\lambda_\chi > \tfrac{1}{4}\lambda_{\chi\phi}^2. \tag{4.2}$$

Together with (4.1a), this also leads to $\lambda_\chi > 0$. As explained in Sec. III, to satisfy the BBN constraint we require that the mass eigenstate Higgs bosons $\hat{\chi}$ and $\hat{\phi}$ predominantly decay into the visible SM particles. This means that the mixings between $\chi - \phi'$ and $\phi - \phi'$ should be sufficiently small. So, inspecting the scalar mass matrix in (2.21) and (2.22), we require the mixing elements $(m_{\phi\phi'}^2, m_{\phi'\chi}^2) \simeq 0$, which impose the following constraints:

$$\lambda_\phi^+ - \lambda_\phi^- \simeq 0, \tag{4.3a}$$

$$\lambda_{\chi\phi}v_\chi - \beta_{\chi\phi} \simeq 0. \tag{4.3b}$$

We find that for the invisible decays of $\hat{\chi}$ and $\hat{\phi}$ into mirror particles to have a branching fraction less than 5–10%, it is enough to numerically hold the conditions (4.3a) and (4.3b) just to a few-percent level.

Since the constraint (3.51) gives $v_\phi > v_{\phi'}$ and the condition (4.1a) shows $\lambda_\phi^+ > 0$, the solution (2.15a) will then require the trilinear coupling $\beta_{\chi\phi}$ to be negative. Combining this with the relation (4.3b), we thus arrive at

$$\beta_{\chi\phi} < 0, \tag{4.4a}$$

$$\lambda_{\chi\phi} < 0, \tag{4.4b}$$

where we have adopted the convention with all Higgs VEVs being positive.

Among eight free parameters in the original Higgs potential (2.8a) and (2.8b), three of them $(\mu_\phi, \mu_\chi, \beta_{\chi\phi})$ have mass dimension equal to 1 and the soft-breaking parameter β_χ has mass dimension equal to 3, while the

other four are dimensionless couplings (λ_ϕ^+, λ_ϕ^-, λ_χ, $\lambda_{\chi\phi}$). The three Higgs VEVs (v_ϕ, $v_{\phi'}$, v_χ) are all constrained by the vacuum conditions (2.18a)–(2.18c) and (2.20). In the above, we have imposed four physical constraints: (i) the Higgs VEV $v_\phi \simeq 174$ GeV is to generate full electroweak symmetry breaking in the visible sector; (ii) the mirror Higgs VEV $v_{\phi'}$, besides realizing the mirror electroweak symmetry breaking, should obey the BBN constraint (3.50) , and we will set a natural sample value $x \equiv v_\phi/v_{\phi'} = 2$ for convenience of the numerical analysis in Sec. IV; (iii) the two additional constraints, $(m^2_{\phi\phi'}, m^2_{\phi'\chi}) \simeq 0$, will ensure the mass eigenstates $\hat{\chi}$ and $\hat{\phi}$ to predominantly decay into the particles in the visible sector (rather than mirror sector). These four constraints will reduce the eight free parameters of the Higgs potential (2.8) down to four, which we may choose, for instance, to be the four dimensionful parameters (μ_ϕ, μ_χ, $\beta_{\chi\phi}$, β_χ). Using (μ_ϕ, μ_χ, $\beta_{\chi\phi}$, β_χ) as inputs, we can then resolve the remaining four parameters in (2.8a) as follows:

$$\lambda_\phi^+ \simeq \lambda_\phi^- \simeq \frac{\mu_\phi^2}{v_\phi^2}\frac{x^2}{x^2+3}, \tag{4.5a}$$

$$\lambda_{\chi\phi} \simeq \frac{\beta_{\chi\phi}}{v_\chi} \simeq -\frac{\beta_{\chi\phi}^2}{2\mu_\phi^2}\frac{x^2+3}{x^2-1}, \tag{4.5b}$$

$$\lambda_\chi \simeq \frac{\mu_\chi^2}{v_\chi^2}\left(1+\frac{\beta_{\chi\phi}^2 v_\phi^2}{\mu_\chi^2\mu_\phi^2}\frac{x^2+3}{x^2-1}\right) - \frac{\beta_\chi}{v_\chi^3}, \tag{4.5c}$$

where the VEV of χ is derived from (2.15a) and (4.5a),

$$v_\chi \simeq \frac{2\mu_\phi^2}{-\beta_{\chi\phi}}\frac{x^2-1}{x^2+3}, \tag{4.6}$$

which is positive due to $x > 1$ and $\beta_{\chi\phi} < 0$. As expected, we see that under the physical constraints, all four dimensionless couplings (λ_ϕ^+, λ_ϕ^-, λ_χ, $\lambda_{\chi\phi}$) are now expressed as functions of the four dimensionful parameters (μ_ϕ, μ_χ, $\beta_{\chi\phi}$, β_χ) of (2.8), in addition to the physically constrained Higgs vacuum expectation value v_ϕ and the ratio $x \equiv v_\phi/v_{\phi'}$. The above analytical solutions will hold to a numerical precision of a few percent for our viable parameter space. Although we will use the exact numerical solutions for the phenomenological analyses below, the above allows us to analytically understand the viable parameter space and provides us with nontrivial consistency checks.

We also note that under the approximation $(m^2_{\phi\phi'}, m^2_{\phi'\chi}) \simeq 0$, the scalar mass matrix (2.21) reduces to a 2×2 matrix form with $\phi - \chi$ mixing,

$$\mathcal{M}^2_{\phi\chi} = \begin{pmatrix} m^2_{\phi\phi} & m^2_{\phi\chi} \\ m^2_{\phi\chi} & m^2_{\chi\chi} \end{pmatrix}. \tag{4.7}$$

Using the approximate condition (4.3), we simplify the elements of mass matrix (4.7) as

$$\begin{aligned} m^2_{\phi\phi} &\simeq \mu_\phi^2\frac{8x^2}{x^2+3}, \\ m^2_{\chi\chi} &\simeq \mu_\chi^2 + v_\phi^2\frac{\beta_{\chi\phi}^2}{2\mu_\phi^2}\frac{x^2+3}{x^2-1}\left(\frac{5x^2-1}{2x^2}+\frac{3}{2}\frac{\beta_\chi}{\beta_{\chi\phi}v_\phi^2}\right), \\ m^2_{\phi\chi} &\simeq 2\beta_{\chi\phi}v_\phi. \end{aligned} \tag{4.8}$$

The mass matrix $\mathcal{M}^2_{\phi\chi}$ can be diagonalized by an orthogonal rotation from the gauge eigenbasis (ϕ, χ) to the mass eigenbasis ($\hat{h}$, $\hat{\chi}$), where the rotation angle θ_χ is given by

$$\sin(2\theta_\chi) = \frac{2m^2_{\phi\chi}}{m^2_{\chi\chi} - m^2_{\phi\phi}}. \tag{4.9}$$

Then we can readily derive the approximate mass eigenvalues for all three Higgs bosons ($\hat{h}$, $\hat{h}'$, $\hat{\chi}$),

$$m^2_{h,\chi} \simeq \frac{1}{2}\left[(m^2_{\phi\phi}+m^2_{\chi\chi}) \pm \sqrt{(m^2_{\phi\phi}-m^2_{\chi\chi})^2+4m^4_{\phi\chi}}\right], \tag{4.10a}$$

$$m^2_{h'} \simeq \mu_\phi^2\frac{8}{x^2+3}, \tag{4.10b}$$

where in (4.10a) the larger (smaller) mass eigenvalue corresponds to the $+(-)$ sign in the bracket. These analytical formulas will be used for consistency checks of our exact numerical samples in Sec. IV.

B. Higgs mass spectrum and couplings: Three numerical samples

With the guidelines from Sec. IV, we can construct realistic numerical samples of our model predictions. Inspecting (4.5a) and (4.6) and setting the ratio $x \equiv v_\phi/v_{\phi'} = 2$, we have

$$v_\chi \simeq \frac{2\lambda_\phi^- v_\phi^2}{-\beta_{\chi\phi}}\frac{x^2-1}{x^2} \simeq \frac{v_\phi^2}{\frac{2}{3}|\beta_{\chi\phi}|/\lambda_\phi^-}. \tag{4.11}$$

So, for the natural choice of $|\beta_{\chi\phi}|/\lambda_\phi^- = O(v_\phi)$, we have $v_\chi = O(v_\phi) = O(v_\phi - v_{\phi'})$. This means that the visible and mirror electroweak symmetry breakings together with the spontaneous mirror parity violation all naturally happen at the weak scale, around $O(10^2$ GeV). Furthermore, for all quartic Higgs couplings $\lambda_i \lesssim O(0.1$–$1)$ in perturbative region of the Higgs potential (2.8), we expect that the three Higgs bosons (ϕ, ϕ', χ) should have masses around $O(10^2$ GeV), which are significantly below 1 TeV.

To avoid the BBN constraint in Sec. III, we have required the two Higgs mass eigenstates $\hat{\chi}$ and $\hat{\phi}$ to predominantly decay into the visible sector. (Hereafter, for convenience we will use the notations $\hat{h}$, $\hat{h}'$, and $\hat{\chi}$ to denote the mass eigenstates of ϕ, ϕ', and χ, respectively, unless specified otherwise.) Numerically, we find it sufficient to have the branching ratios of $\hat{\chi}$ and $\hat{h}$ decays into the visible sector larger than about 90%. So more than 90%

TABLE I. Three samples of input parameters for the Higgs potential (2.8) in our model.

Sample	μ_ϕ (GeV)	μ_χ (GeV)	$\beta_{\chi\phi}$ (GeV)	λ_ϕ^-	λ_ϕ^+	$\lambda_{\chi\phi}$	λ_χ	$\beta_\chi^{1/3}$ (GeV)
A	70	113	−35	0.094	0.0923	−0.28	2.03	−30
B	60	255	−21	0.068	0.0696	−0.154	3.42	−30
C	62	56.6	−5	0.077	0.0747	−0.0074	0.0075	−20

of the vacuum energies associated with $\hat{\chi}$ and $\hat{h}$ will be converted to the visible sector and less than 10% to the mirror sector. Thus the temperature T of the visible sector will be reheated up to $T \propto (90\%)^{(1/4)} \max(v_\chi, v_\phi) \simeq 0.97 \max(v_\chi, v_\phi)$, and the T' of the mirror sector will be reheated up to $T' \propto (10\%)^{(1/4)} \max(v_\chi, v_\phi) \simeq 0.56 \max(v_\chi, v_\phi)$ due to the $\hat{\chi}$ and $\hat{h}$ decays. This leads to a ratio $T'/T \sim 0.58$, which still obeys the BBN constraint (3.46).

Taking all these into consideration, we systematically explore the viable parameter space via numerical analysis. To cover the main parameter space, we have constructed three sample inputs, called sample-A, -B, and -C, respectively, which are summarized in the Table I. We see that the mass parameters μ_ϕ and μ_χ, as well as the dimensionful cubic coupling (over the dimensionless quartic couplings $\lambda_\phi^\pm$), $\beta_{\chi\phi}/\lambda_\phi^\pm$, are all of $O(10^2$ GeV). The four quartic Higgs couplings are in the natural range of $O(1$–$0.01)$.

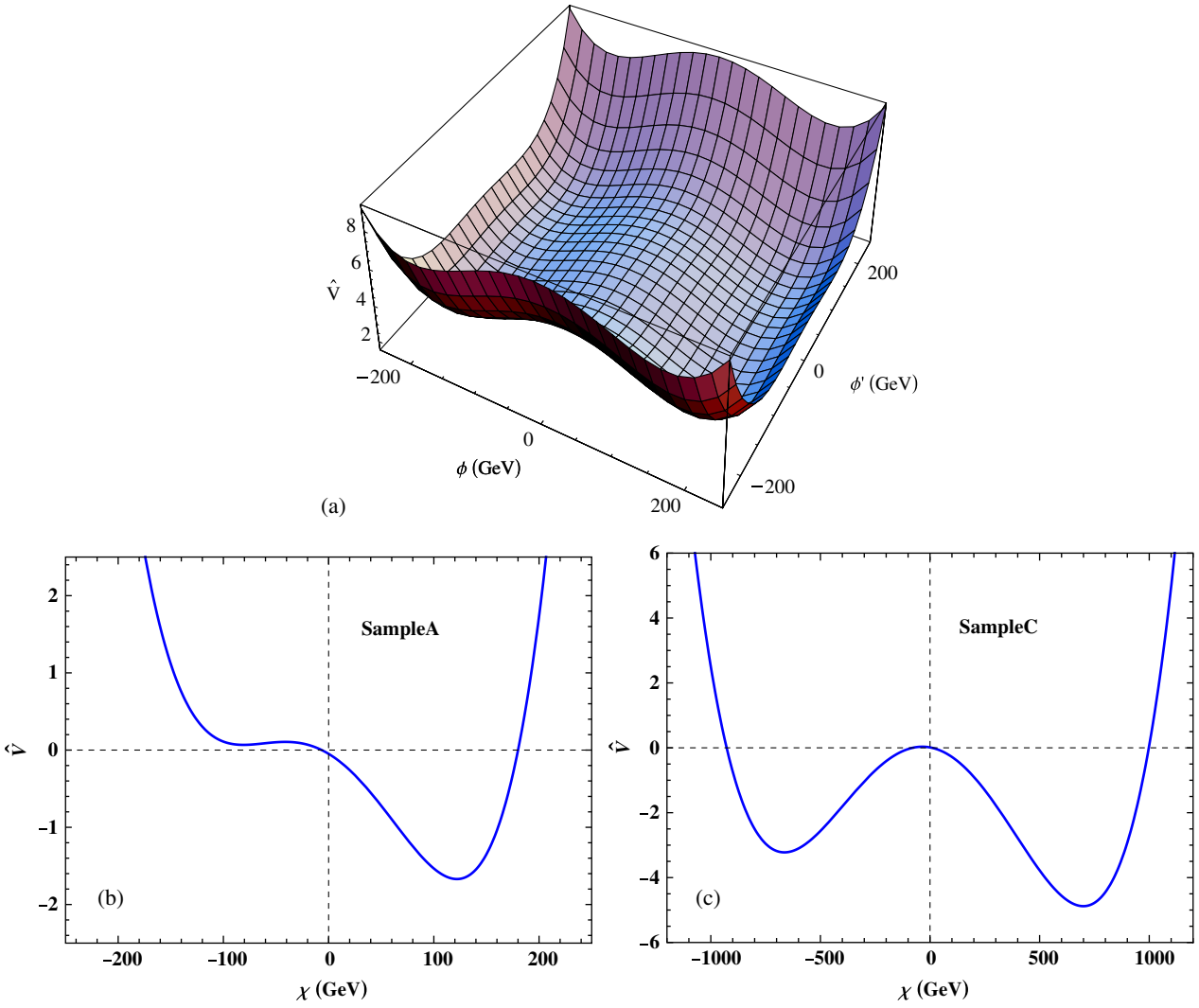

FIG. 1 (color online). Vacuum structure of the Higgs potential V. The plot in (a) depicts $\hat{V}$ as a function of ϕ and ϕ', for sample-A; and the features for sample-B and -C appear very similar. The plot in (b) displays the potential V in the same units as a function of χ in sample-A, while (c) shows V versus χ in sample-C. The potential $\hat{V}$ is in units of 10^8 GeV^4.

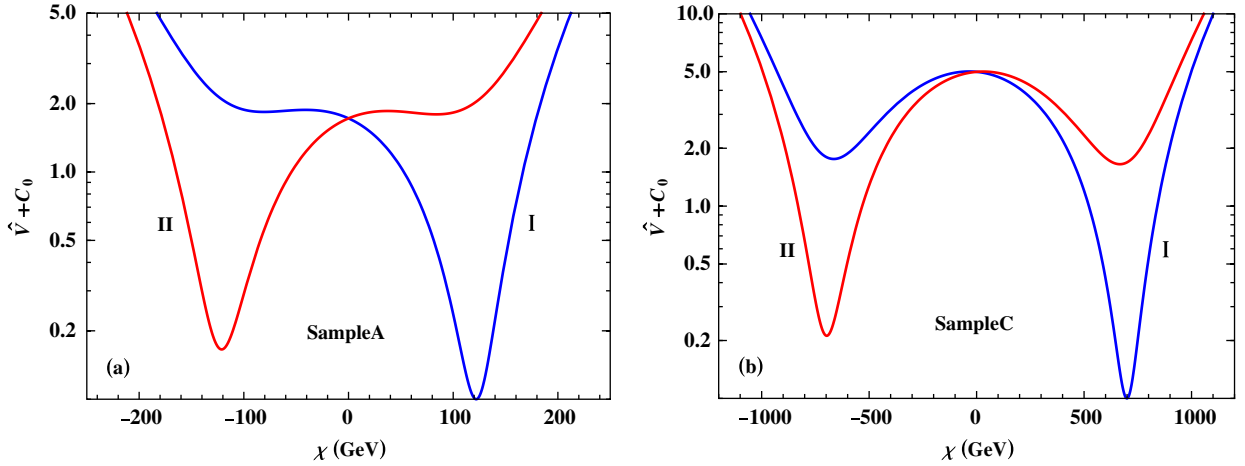

FIG. 2 (color online). Nondegenerate vacua of the Higgs potential $\hat{V}$ due to minimal soft breaking. The plot in (a) depicts V as a function of χ for sample-A and (b) is for sample-C. In each plot, the curve-I (blue) represents $\hat{V}(\phi, \phi', \chi)$ and the curve-II (red) denotes $\hat{V}(\phi', \phi, \chi)$. For convenience of plotting, a pure constant shift C_0 is added to $\hat{V}$ (cf. text). The potential V is in unit of 10^8 GeV^4.

In Fig. 1, we analyze the vacuum structure of the Higgs potential V in (2.8) or (2.11). For Fig. 1(a), we display the Higgs potential $\hat{V}$ as a function of visible and mirror Higgs fields, ϕ and ϕ', where $\hat{V}$ is plotted in units of 10^8 GeV^4 and the singlet scalar χ is set to its extremal value v_χ. Here we choose sample-A as an example for illustration, but we find that the features of sample-B and -C appear very similar to Fig. 1(a). We see that the potential minimum occurs at $(|\phi|, |\phi'|) = (v_\phi, v_{\phi'}) = (174, 87)$ GeV, with a ratio $v_\phi/v_{\phi'} = 2$. In Figs. 1(b) and 1(c) we depict the Higgs potential V (in unit of 10^8 GeV^4) as a function of the P-odd singlet Higgs field χ, for sample-A and -C, respectively. In these two plots, we have set the other two Higgs fields ϕ and ϕ' to their extremal values $(v_\phi, v_{\phi'})$. Note that the two minima in the potential are asymmetric for χ, and the true minimum is given by the right one with $v_\chi = 122$ GeV in sample-A and $v_\chi = 699$ GeV in sample-C. This is expected because the asymmetry is generated by the unique cubic term, $\beta_{\chi\phi}(|\phi| - |\phi'|^2)\chi$, in the Higgs potential (2.8a), which is *linear* in χ and realizes the spontaneous mirror parity violation. Since $\beta_{\chi\phi} < 0$ and $v_\phi > v_{\phi'}$, we see that this cubic term becomes positive for $\chi < 0$ and negative for $\chi > 0$. This explains why in Fig. 1(b) and 1(c) the right minimum is lower than the left one, and thus serves as the true minimum of the potential. The asymmetry between the two minima in Fig. 1(b) is much larger than that in Fig. 1(c), because the size of the cubic coupling $|\beta_{\chi\phi}|$ in sample-A is a factor of 7 bigger than that in sample-C (cf. Table I). In addition, we have made the same plot of $\hat{V}$ versus χ for sample-B and find its shape is between Fig. 1(b) and Fig. 1(c), so we do not display sample-B here.

We note that there are two degenerate field configurations in the vacuum potential (2.11b),

$$\langle V(\phi, \phi', \chi)\rangle = \langle V(\phi', \phi, -\chi)\rangle, \tag{4.12}$$

and they transform into each other under mirror parity. But due to the minimal soft-breaking term $\langle \Delta\hat{V}_{\rm soft}\rangle$ in (2.11c), these two vacuum states become nondegenerate, and the full potential $\langle\hat{V}\rangle$ splits between these two vacuum configurations,

$$\langle\hat{V}(\phi, \phi', \chi)\rangle - \langle\hat{V}(\phi', \phi, -\chi)\rangle = 2\langle\Delta\hat{V}_{\rm soft}(\chi)\rangle. \tag{4.13}$$

So this provides the simplest way to evade the domain-wall problem. To explicitly check the nondegeneracy between the two vacuum configurations under soft breaking (2.11c), we plot $\hat{V}(\phi, \phi', \chi)$ and $\hat{V}(\phi', \phi, \chi)$ in Fig. 2 as curve-I (blue) and curve-II (red), respectively. The Fig. 2(a) is for sample-A and Fig. 2(b) is for sample-C. The potential $\hat{V}$ is in unit of 10^8 GeV^4, and for convenience of plotting we have shifted the potential $\hat{V}$ by a pure constant $C_0 = 1.77 \times 10^8$ GeV^4 ($C_0 = 4.98 \times 10^8$ GeV^4) in Fig. 2(a) [Fig. 2(b)]. It is clear that in each plot the minima of curve-I and curve-II are no longer degenerate, and the true vacuum minimum is given by the one in curve-I.

Next, we systematically derive the outputs for all three samples, as summarized in Table II. For each sample, we solve the global minimum of the Higgs potential $\hat{V}$ numerically, and thus determine the three vacuum expectation values $(v_\phi, v_{\phi'}, v_\chi)$. From Table II, the Higgs vacuum expectation value $v_\phi = 174$ GeV just generates the observed electroweak symmetry breaking in the visible sector, while $v_{\phi'} = v_\phi/2$ holds for all three samples. So they all give the same prediction for the mirror dark matter density according to (3.32). The VEV of the P-odd Higgs singlet χ significantly varies among the three samples, it is around $O(v_\phi)$ in sample-A and -B, but is about a factor of 4 larger than v_ϕ in sample-C.

We further diagonalize the 3×3 Higgs mass matrix (2.21) and (2.22) for each sample, and derive their mass

TABLE II. Outputs of the three samples, including all Higgs VEVs and Higgs masses, in units of GeV. The three mixing elements $U_{\phi h}$, $U_{\phi h'}$, and $U_{\phi\chi}$ in the rotation matrix U are also listed, which characterize the transformations of ϕ into the mass eigenstate $\hat{h}$, $\hat{h}'$, and $\hat{\chi}$, respectively.

Sample	v_ϕ	$v_{\phi'}$	v_χ	m_h	$m_{h'}$	m_χ	$U_{\phi h}$	$U_{\phi h'}$	$U_{\phi\chi}$
A	174	87	122	122	75.1	203	0.841	0.0063	−0.541
B	174	87	147	125	64.5	277	0.992	−0.0068	−0.125
C	174	87	699	136	67.8	59.4	0.993	0.0062	+0.119

eigenvalues as shown in Table II. All three samples have a SM-like Higgs boson $\hat{h}$, with masses falling into the range 120–140 GeV; while the Higgs boson $\hat{h}'$ is mainly from the mirror Higgs doublet ϕ' and has a mass around 67–75 GeV, which is about half of the $\hat{h}$ mass. This is quite expected since we have the ratio of two-Higgs-doublet VEVs, $v_\phi/v_{\phi'} = 2$, based upon the condition (3.51). Finally, for the Higgs boson $\hat{\chi}$, we have $m_\chi < 2m_h$ in sample-A, and $m_\chi > 2m_h$ in sample-B. But, in contrast with both sample-A and -B, sample-C has $m_\chi < \frac{1}{2}m_h$. As will be shown in Sec. VI, these three samples will lead to distinctive new Higgs signatures for the LHC discovery.

For diagonalizing the 3×3 Higgs mass matrix $\mathcal{M}^2$ in (2.21) and (2.22), we introduce the orthogonal rotation matrix U, which connects the gauge eigenbasis (ϕ, ϕ', χ) to the mass eigenbasis $(\hat{h}, \hat{h}', \hat{\chi})$. So we have $U^T\mathcal{M}^2U = \mathcal{D}^2$, where the diagonal mass matrix $\mathcal{D}^2 = \mathrm{diag}(m_\phi^2, m_{\phi'}^2, m_\chi^2)$. The predicted mass eigenvalues are summarized in Table II, and we derive the rotation matrix U for all three samples as follows:

$$\text{sample-A:}\quad U = \begin{pmatrix} 0.8408 & 0.006\,30 & -0.5413 \\ -0.005\,34 & 1 & 0.003\,35 \\ 0.5413 & 0.000\,07 & 0.8408 \end{pmatrix}, \tag{4.14a}$$

$$\text{sample-B:}\quad U = \begin{pmatrix} 0.9921 & -0.006\,79 & -0.1254 \\ 0.006\,58 & 1 & -0.002\,12 \\ 0.1254 & 0.001\,28 & 0.9921 \end{pmatrix}, \tag{4.14b}$$

$$\text{sample-C:}\quad U = \begin{pmatrix} 0.9929 & 0.006\,17 & 0.1187 \\ -0.009\,77 & 0.9995 & 0.0298 \\ -0.1184 & -0.0307 & 0.9925 \end{pmatrix}. \tag{4.14c}$$

We see that the (1, 3) element $U_{\phi\chi}$, which characterizes the mixing between ϕ and χ, is 54.1%, 12.5%, and 11.9% in sample-A, -B, and -C, respectively. On the other hand, the (1, 2) element $U_{\phi h'}$ and (2, 3) element $U_{\phi'\chi}$ represent mixings between $\phi - \phi'$ and $\phi' - \chi$, respectively; they are always around 2–3% or smaller for the three samples; so they are negligible for our phenomenology studies below. Furthermore, the (1, 1) element $U_{\phi h}$ describes the transition of ϕ into its mass eigenstate $\hat{h}$; this equals 84% in sample-A, and is more than 99% in both sample-B and -C. It is clear that the mass eigenstate $\hat{h}$ mainly arises from visible Higgs doublet ϕ, while the mass eigenstate $\hat{\chi}$ largely comes from χ and has sizable mixings with ϕ. For comparison we summarize these three elements of U into the last columns of Table II.

Then, using the mixing matrix (4.14) we further derive all the mass eigenbasis couplings of Higgs bosons with themselves, with the gauge bosons, and with the fermions, respectively. These are summarized in Tables III and IV. For all cubic scalar couplings in Table III, we have factorized out a common dimension-1 VEV parameter, $v = \sqrt{2}v_\phi \simeq 246$ GeV, and the numbers shown are all dimensionless.

In Table IV, we use V to represent the visible weak gauge bosons ($W^\pm$, Z^0), while V' denotes their mirror partners ($W^{\pm\prime}$, $Z^{0\prime}$). Similarly, we use f and f' to denote ordinary fermions (either quark or lepton) and mirror fermions, respectively. For $\hat{h}VV$, $\hat{\chi}VV$, and $\hat{h}'V'V'$ couplings, we have divided them by a common coupling (taken as the SM value of $\hat{h}VV$ coupling); while for $\hat{h}f\bar{f}$, $\hat{\chi}f\bar{f}$ and $\hat{h}'f'\bar{f}'$ couplings, we divide them by a common coupling (chosen as the SM value of $\hat{h}f\bar{f}$ coupling). We see that the $\hat{h}$ couplings to gauge bosons and to fermions have significant deviation (16%) from the SM values in sample-A, while those in sample-B and -C are fairly close to the corresponding SM values. But the $\hat{\chi}$ couplings to gauge bosons and to fermions vary a lot among the three samples. Relative to the SM value of $\hat{h}VV$ or $\hat{h}f\bar{f}$ coupling, the largest $\hat{\chi}VV$ or

TABLE III. Predicted Higgs boson self-couplings in the mass eigenbasis, where for the trilinear couplings we have factorized out a common VEV parameter, $v = \sqrt{2}v_\phi \simeq 246$ GeV, so the listed numbers are all dimensionless.

Sample	$\hat{\chi}\hat{\chi}\hat{\chi}$	$\hat{\chi}\hat{\chi}\hat{h}$	$\hat{\chi}\hat{h}\hat{h}$	$\hat{h}\hat{h}\hat{h}$	$\hat{\chi}\hat{\chi}\hat{\chi}\hat{\chi}$	$\hat{\chi}\hat{\chi}\hat{\chi}\hat{h}$	$\hat{\chi}\hat{\chi}\hat{h}\hat{h}$	$\hat{\chi}\hat{h}\hat{h}\hat{h}$	$\hat{h}\hat{h}\hat{h}\hat{h}$
A	0.586	1.360	0.429	0.182	0.243	0.653	0.704	0.184	0.052
B	2.010	0.713	−0.058	0.126	0.829	0.428	0.048	−0.019	0.033
C	0.020	−0.009	0.035	0.151	0.002	−0.001	0.002	0.018	0.037

TABLE IV. Predicted Higgs couplings with visible/mirror gauge bosons and fermions. We use $V(=W^{\pm}, Z^0)$ and f to denote the visible weak gauge bosons and fermions (either quark or lepton), respectively, while V' and f' are their corresponding mirror partners. For $\hat{h}VV$, $\hat{\chi}VV$, and $\hat{h}'V'V'$ couplings, we have divided them by a common coupling which equals the SM value of the $\hat{h}VV$ coupling; similarly, for $\hat{h}f\bar{f}$, $\hat{\chi}f\bar{f}$, and $\hat{h}'f'\bar{f}'$ couplings, we divide them by a common coupling which equals the SM value of the $\hat{h}f\bar{f}$ coupling.

Sample	$\hat{h}VV$	$\hat{\chi}VV$	$\hat{h}f\bar{f}$	$\hat{\chi}f\bar{f}$	$\hat{h}'V'V'$	$\hat{h}'f'\bar{f}'$
A	0.841	−0.541	0.841	−0.541	0.5	1
B	0.992	−0.125	0.992	−0.125	0.5	1
C	0.993	0.119	0.993	0.119	0.5	1

$\hat{\chi}f\bar{f}$ coupling is about 54% in sample-A, and reduces to about 13% and 12% in sample-B and -C. The ratio of the mirror coupling $\hat{h}'V'V'$ over the SM value of $\hat{h}VV$ coupling equals $\frac{v_{\phi'}}{v_{\phi}} \simeq \frac{1}{2}$ to high precision, as shown in the sixth column of Table IV, where the invoked gauge couplings cancel in this ratio because the mirror parity requires identical gauge couplings between the visible and mirror gauge groups. Furthermore, all mirror Yukawa couplings equal the corresponding SM Yukawa couplings, so the last column of Table IV has little deviation from 1 since the element $U_{\phi' h'} \simeq 1$ holds to high accuracy and the mixings of $\hat{h}'$ with the other two Higgs bosons are negligible in our model, as shown in (4.14). This also means that the ratio of every mirror fermion mass over the corresponding SM fermion mass is given by $\frac{m_{f'}}{m_f} \simeq \frac{v_{\phi'}}{v_{\phi}} \simeq \frac{1}{2}$, to good precision in the present model. Finally, we note that the masses of visible and mirror weak gauge bosons obey the relation $\frac{M_{V'}}{M_V} = \frac{v_{\phi'}}{v_{\phi}}$, where $V = (W, Z)$ and $V' = (W', Z')$.

C. Low-energy precision constraints

Inspecting Table II, we see that the mirror Higgs boson $\hat{h}'$ is rather light in all three samples, around 67–75 GeV, while the singlet Higgs boson $\hat{\chi}$ becomes the lightest scalar of mass about 59 GeV in sample-C. It is thus important to analyze the lower energy direct and indirect precision constraints on our model.

For the mirror Higgs boson $\hat{h}'$, its coupling to the visible gauge bosons WW/ZZ and fermions $f\bar{f}$ could be generated via the $\phi - \phi'$ mixing, i.e., the mixing element $U_{\phi h'} = O(10^{-2})$ in (4.14). The LEP Collaboration [48] has searched for the Higgs boson in the reaction $e^- e^+ \to Zh$ with Higgs decay via $h \to b\bar{b}$. So we can analyze a similar channel for searching the mirror Higgs $\hat{h}'$ at LEP via $e^- e^+ \to Z\hat{h}'$ with $\hat{h}' \to b\bar{b}$. Then, we immediately realize that the production cross section is suppressed by a factor $U^2_{\phi h'}$ and this same factor $U^2_{\phi h'}$ enters again the decay branching fraction of $\hat{h}' \to b\bar{b}$. Hence, the expected final signals of mirror $\hat{h}'$ must be suppressed by a factor of $U^4_{\phi h'}$ relative to that of the SM Higgs boson with the same mass, which is $U^4_{\phi h'} \sim 10^{-9}$ for all three samples. It is clear that the LEP data [48] actually place no bound on such a nearly invisible light mirror Higgs boson.

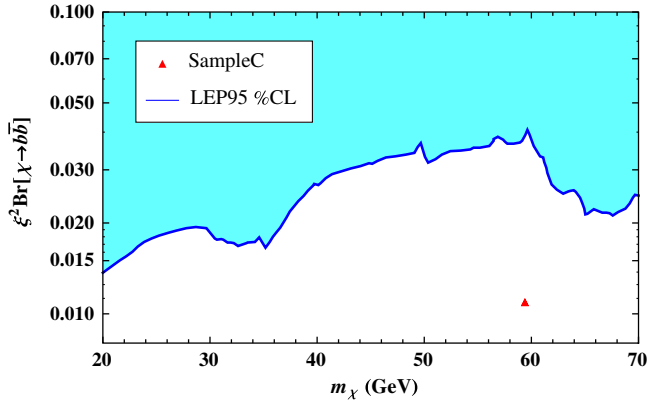

FIG. 3 (color online). The LEP upper bound on the product $\xi^2 \mathrm{Br}[\hat{\chi} \to b\bar{b}]$ is depicted by the blue curve, where the shaded region above the curve is excluded at 95% C.L. The prediction of sample-C is marked by the red triangle.

Then we analyze the possible LEP direct search limit on the P-odd singlet Higgs boson $\hat{\chi}$. Inspecting Table II, we see that the $\hat{\chi}$ mass in sample-A and -B lies in the range of 200–290 GeV, and thus beyond the kinematical capability of LEP. Only sample-C predicts a rather light χ with mass at 59.4 GeV which is potentially accessible by LEP. The relevant reaction for $\hat{\chi}$ detection is via $e^- e^+ \to Z\hat{\chi}$ via the decay $\hat{\chi} \to b\bar{b}$. This channel invokes the $\hat{\chi}ZZ$ and $\hat{\chi}b\bar{b}$ couplings, which are suppressed by the mixing element $U_{\phi\chi}$ in (4.14) relative to the SM couplings of hZZ and $hb\bar{b}$, respectively. So we deduce the following relation for the ratios of $\hat{\chi}$ couplings over the corresponding SM Higgs couplings,

$$\xi \equiv \frac{C_{\chi ZZ}}{C^{\mathrm{SM}}_{hZZ}} = \frac{C_{\chi f\bar{f}}}{C^{\mathrm{SM}}_{hf\bar{f}}} = U_{\phi\chi}. \tag{4.15}$$

For sample-C, we have computed the mixing element $U_{\phi\chi} \simeq 0.12$ as in (4.14), and the decay branching ratio, $\mathrm{Br}[\hat{\chi} \to b\bar{b}] = 80.5\%$, as will be summarized in Table V of the next section. So we can derive a product for sample-C, relevant to the LEP constraint,

$$\xi^2 \mathrm{Br}[\hat{\chi} \to b\bar{b}] = 0.011. \tag{4.16}$$

For any nonstandard Higgs boson, the LEP experimental analysis [48] already puts a nontrivial limit on the product of ξ^2 with the Higgs decay branching fraction into $b\bar{b}$. We display the LEP upper bound [48] in Fig. 3, where the shaded region above the curve is excluded at 95% C.L. and the prediction (4.16) of sample-C is marked as the red triangle. We find that sample-C is fully consistent with the LEP limit.

Next we analyze the indirect electroweak precision constraints on the Higgs sector of our model. The effects of new physics can be generally formulated into the oblique corrections, as characterized by the parameters (S, T, U) [49].

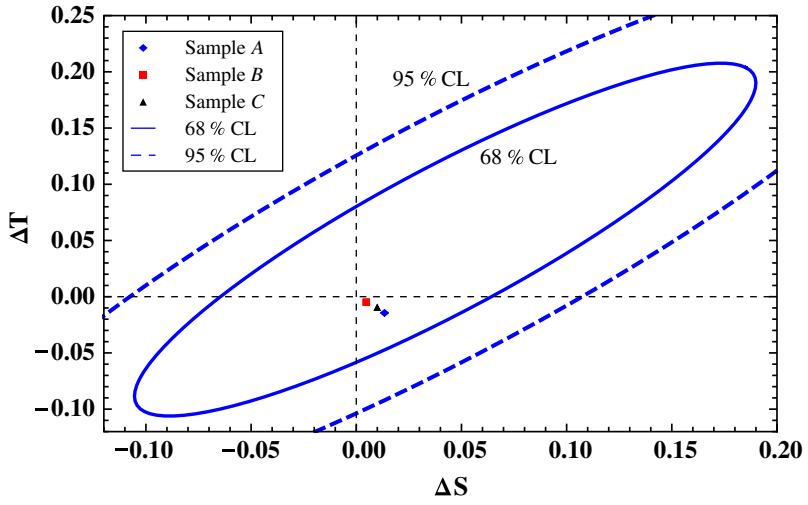

FIG. 4 (color online). The electroweak precision constraints in the $\Delta S - \Delta T$ plane, with a SM reference point $m_h^{\rm ref} = 120$ GeV. The predictions of our sample-A, -B, and -C are marked by the blue diamond, red square, and black triangle, respectively.

Since our model contains light Higgs bosons with masses comparable to the Z mass m_Z, we will adopt a more precise set of formulas to compute the (S, T, U) as in [50]. Thus, for the SM Higgs boson, we have the oblique corrections

$$S_{\rm SM}[m_h] = \frac{1}{\pi}\left[\frac{3m_h^2}{8m_Z^2} - \frac{m_h^4}{12m_Z^4} + \frac{m_h^2}{m_Z^2}\ln\frac{m_h^2}{m_Z^2} \times \left(\frac{3m_Z^2 - m_h^2}{4m_Z^2} + \frac{m_h^4}{24m_Z^4} + \frac{3m_Z^2}{4(m_Z^2 - m_h^2)}\right) + \left(1 - \frac{m_h^2}{3m_Z^2} + \frac{m_h^4}{12m_Z^4}\right)\frac{m_h q(m_h)}{m_Z^2}\right], \quad (4.17a)$$

$$T_{\rm SM}[m_h] = \frac{3}{16\pi s_Z^2 c_Z^2}\left[\frac{m_h^2}{m_Z^2 - m_h^2}\ln\frac{m_h^2}{m_Z^2} - \frac{c_Z^2 m_h^2}{c_Z^2 m_Z^2 - m_h^2}\ln\frac{m_h^2}{c_Z^2 m_Z^2}\right], \quad (4.17b)$$

with the function $q(m_h)$ defined as

$$q(m_h) = \begin{cases} \sqrt{4m_Z^2 - m_h^2}\arctan\frac{\sqrt{4m_Z^2 - m_h^2}}{m_h}, & m_h \le 2m_Z, \\ \sqrt{m_h^2 - 4m_Z^2}\ln\frac{2m_Z}{m_h + \sqrt{m_h^2 - 4m_Z^2}}, & m_h \ge 2m_Z, \end{cases}$$

where the weak mixing angle θ_W is defined at the Z pole, and we use the notations $s_Z^2 = \sin^2\theta_W|_Z$ and $c_Z^2 = 1 - s_Z^2$. The Higgs correction to the oblique parameter U is much smaller and thus negligible in the analysis below. For the case of large Higgs mass $m_h^2 \gg m_Z^2$, it is justified to expand the above formulas. So we can reproduce the conventional approximate results [49] under the large Higgs mass expansion, as a consistency check,

$$S_{\rm SM}[m_h] \approx \frac{1}{12\pi}\ln\frac{m_h^2}{m_Z^2}, \quad (4.18a)$$

$$T_{\rm SM}[m_h] \approx -\frac{3}{16\pi c_Z^2}\ln\frac{m_h^2}{m_Z^2}. \quad (4.18b)$$

In the present mirror model, the three Higgs bosons have mixings in their gauge eigenbasis, and we transform them into the mass eigenbasis via the mixing matrix U in Eq. (4.14). So we can derive the new contributions of all Higgs bosons to S and T,

$$\Delta S = U_{\phi h}^2 S_{\rm SM}[m_h] + U_{\phi h'}^2 S_{\rm SM}[m_{h'}] + U_{\phi\chi}^2 S_{\rm SM}[m_\chi] - S_{\rm SM}[m_h^{\rm ref}], \quad (4.19a)$$

$$\Delta T = U_{\phi h}^2 T_{\rm SM}[m_h] + U_{\phi h'}^2 T_{\rm SM}[m_{h'}] + U_{\phi\chi}^2 T_{\rm SM}[m_\chi] - T_{\rm SM}[m_h^{\rm ref}], \quad (4.19b)$$

where we have subtracted the SM Higgs contributions at the reference point $m_h^{\rm ref}$, and U_{ij} denotes the relevant element of the mixing matrix U.

From (4.19) and (4.17), we explicitly compute the oblique corrections in our mirror model, for the three samples in Table II, and arrive at

$$\text{sample-A:}\quad (\Delta S, \Delta T) = (0.0134, -0.0138), \quad (4.20a)$$

$$\text{sample-B:}\quad (\Delta S, \Delta T) = (0.0048, -0.0043), \quad (4.20b)$$

$$\text{sample-C:}\quad (\Delta S, \Delta T) = (0.0100, -0.0088), \quad (4.20c)$$

where we have set the SM reference point $m_h^{\rm ref} = 120$ GeV. Then, we analyze the electroweak precision data [51] and make a precision fit by using the method of Peskin and Wells [52]. We choose the three most accurately measured observables [51], $\Gamma_\ell[Z]$, M_W, and $\sin^2\theta_W^{\rm eff}$, for the precision $\Delta S - \Delta T$ fit with $\Delta U = 0$ and the SM reference point $m_h^{\rm ref} = 120$ GeV. For computing the SM contributions, we have followed the approach of Marciano [53] and take into account the allowed experimental ranges of the top mass m_t and fine structure constant $\alpha(m_Z)$ [51]. The resultant constraints on $\Delta S - \Delta T$ are shown in Fig. 4 at 68% C.L. and 95% C.L., respectively. Our precision fit is in good agreement with the recent more elaborated systematical analysis by the Gfitter Group [54]. In Fig. 4, we

have marked the predictions (4.20) of our sample-A, -B, and -C by the blue diamond, red square, and black triangle, respectively. We see that they are fully consistent with the precision constraints.

Finally, we analyze the low-energy precision constraint on the kinetic mixing parameter ϵ in (2.6). For the case with unbroken mirror parity, the electroweak scales are exactly the same in the two sectors ($v_\phi = v_{\phi'}$) as in [17]. It was suggested by Carlson and Glashow that this mixing can be probed through the oscillations of orthopositronium (o-Ps) and mirror orthopositronium (o-Ps$'$). The oscillation effect becomes maximal when o-Ps and o-Ps$'$ have the same masses. But this does not apply to the case with spontaneously broken mirror parity ($v_\phi \neq v_{\phi'}$). If $v_\phi \ll v_{\phi'}$ as realized in [7], there is basically no constraint available. But, for $v_\phi \gtrsim v_{\phi'}$ as realized in our construction, we can derive a nontrivial limit from the invisible decays of the o-Ps. The visible decays of o-Ps mainly go to 3γ channel, and the decay width is given by [55]

$$\Gamma[\text{o-Ps} \to 3\gamma] \simeq 4.63 \times 10^{-18}\ \text{GeV}, \tag{4.21}$$

which represents the total width to good accuracy. The SM can provide invisible decays of orthopositronium via o-Ps $\to \nu_e \bar{\nu}_e$, which has a partial decay width [55],

$$\Gamma[\text{o-Ps} \to \nu_e \bar{\nu}_e] = \frac{G_F^2 \alpha^3 m_e^5}{24\pi^2}(1 + 4\sin^2\theta_W)^2 \simeq 2.88 \times 10^{-35}\ \text{GeV}, \tag{4.22}$$

and thus the corresponding branching fraction, Br[o-Ps $\to \nu_e \bar{\nu}_e] \simeq 6.22 \times 10^{-18}$. This is negligibly small as it is far below the present experimental upper bound on the branching ratio of all possible invisible decays [20],

$$\text{Br}[\text{o-Ps} \to \text{invisible}] < 4.2 \times 10^{-7}, \tag{4.23}$$

which holds at 90% C.L.

In our model, the mirror-particle-induced invisible decays of o-Ps predominantly go to mirror electron-positron pairs, o-Ps $\to e'^+ e'^-$. So, we can compute its partial decay width,

$$\Gamma[\text{o-Ps} \to e'^- e'^+] = \frac{16\pi\alpha^2\epsilon^2}{3}\frac{|\psi(0)|^2}{M^2} \times \left(1 + \frac{m_{e'}^2}{2m_e^2}\right)\sqrt{1 - \frac{m_{e'}^2}{m_e^2}}, \tag{4.24}$$

where $M \simeq 2m_e$ is the mass of o-Ps, and $|\psi(0)|^2 = \frac{\alpha^3 m_e^3}{8\pi}$ is the square of the wave function at the origin. For the spontaneous mirror parity violation, we have $\frac{m_e}{m_{e'}} = \frac{v_\phi}{v_{\phi'}} \equiv x$. So, from (4.21) and (4.24), we can derive the branching fraction of the invisible decay channel o-Ps $\to e'^+ e'^-$,

$$\text{Br}[\text{o-Ps} \to e'^- e'^+] \simeq 379.3\epsilon^2\left(1 + \frac{1}{2x^2}\right)\sqrt{1 - \frac{1}{x^2}}, \tag{4.25}$$

which is proportional to ϵ^2. Following our numerical samples in Sec. IV, we have $x = \frac{v_\phi}{v_{\phi'}} = 2$, and thus $m_e = 2m_{e'}$. So, from the experimental limit (4.23), we can infer the upper bound of ϵ at 90% C.L.,

$$\epsilon < 3.4 \times 10^{-5}. \tag{4.26}$$

V. NEW HIGGS SIGNATURES AT THE LHC

In this section, we further derive decay widths and branching fractions of the nonstandard Higgs bosons in the present model. We identify their major LHC production and decay channels then we analyze the predictions for new Higgs signatures at the LHC. As shown in the previous section, our mirror model construction generically predicts light Higgs bosons with distinct mass spectrum and nonstandard couplings. Especially, the P-odd scalar $\hat{\chi}$, characterizing spontaneous mirror parity violation, has a mass equal 277 GeV in sample-B, which is more than twice of the mass $m_h = 125$ GeV of the SM-like Higgs boson $\hat{h}$; while $\hat{\chi}$ is as light as about 59 GeV for sample-C and is less than half of the $\hat{h}$ mass of 136 GeV. Note that ϕ can also have sizable mixing with χ, which is about 54.1%, 12.5%, and 11.9% in sample-A, -B, and -C, respectively. These will lead to new Higgs production and decay channels, and can be experimentally searched at the LHC. In addition, the mirror Higgs boson $\hat{h}'$ in our construction is always light, with a mass around 67–75 GeV, which is about half of the $\hat{h}$ mass due to the VEV ratio of $v_{\phi'}/v_\phi = \frac{1}{2}$. But, as the mixing of $\hat{h}'$ with $\hat{h}$ and $\hat{\chi}$ is always below 2–3%, it largely decouples from the visible sector and dominantly decays into invisible mirror partners. The distinct features above also make our Higgs phenomenology fully different from all previous mirror models in the literature [56–58]. For instance, our model always forbids mirror Higgs $\hat{h}'$ decays into visible Higgs $\hat{h}$ via $\hat{h}' \to \hat{h}\,\hat{h}$, while the inverse channel, $\hat{h} \to \hat{h}'\hat{h}'$, is either disallowed or practically negligible.

Based on the Higgs mass spectrum in Table II and Higgs couplings in Tables III and IV, we systematically compute the Higgs decay widths and branching fractions. These results are summarized in Table V. As shown in (4.14), the mixing of the mirror Higgs boson $\hat{h}'$ with $\hat{h}$ or $\hat{\chi}$ is always below about 2–3% and thus negligible for the current analysis, so we do not to list the $\hat{h}'$ decays in Table V. Also, we find that invisible decays of $\hat{h}$ and $\hat{\chi}$ into the mirror gauge bosons or fermions are much suppressed and always below 4%, which are not useful for the current Higgs searches at the LHC. So for clarity of Table V, we omit them as well. We further note that the Higgs $\hat{h}$ in sample-C has a new on-shell decay channel with Br$[\hat{h} \to \hat{\chi}\,\hat{\chi}] = 10\%$, and the Higgs $\hat{\chi}$ in sample-B has the new channel with Br$[\hat{\chi} \to \hat{h}\,\hat{h}] = 11\%$. This means that their branching fractions have sizable deviations from those of the SM Higgs boson with the same mass. For the other four cases in Table V, the

TABLE V. Total decay widths and major decay branching fractions of Higgs bosons $\hat{h}$ and $\hat{\chi}$ in sample-A, -B, and -C. For WW and ZZ decay channels. For WW and ZZ decay channels, the numbers marked by a superscript * denote that one of the weak gauge boson in the final state is off-shell.

Sample	A		B		C	
Higgs	$\hat{h}$	$\hat{\chi}$	$\hat{h}$	$\hat{\chi}$	$\hat{h}$	$\hat{\chi}$
Γ (MeV)	2.63	454	4.10	110	7.49	0.0226
WW	0.157*	0.728	0.209*	0.615	0.358*	0
ZZ	0.0185*	0.268	0.0263*	0.269	0.0499*	0
$\hat{h}\hat{h}$	0	0	0	0.113	0	0
$\hat{\chi}\hat{\chi}$	0	0	0	0	0.102	0
$b\bar{b}$	0.617	0.0022	0.565	6.4×10^{-4}	0.332	0.805
$\tau\bar{\tau}$	0.0672	2.7×10^{-4}	0.0619	8.2×10^{-5}	0.0369	0.0759
$c\bar{c}$	0.0311	1.1×10^{-4}	0.0285	3.2×10^{-5}	0.0167	0.0411
gg	0.0866	9.0×10^{-4}	0.0843	5.7×10^{-4}	0.0593	0.0284
$\gamma\gamma$	0.0022	5.2×10^{-5}	0.0023	1.5×10^{-5}	0.0018	4.4×10^{-4}
$Z\gamma$	0.0012	1.7×10^{-4}	0.0015	6.3×10^{-5}	0.0020	0

branching fractions of $\hat{h}$ or $\hat{\chi}$ appear quite similar to those of the SM Higgs boson, up to a few percent of corrections due to their invisible decays into mirror partners. But in all cases of Table V, the decay widths can significantly differ from the SM due to the relevant suppression factor U_{ij}^2 from the mixing matrix (4.14).

To derive Higgs decay width, we have included QCD radiative corrections. For $q\bar{q}$ final state, the leading-order Higgs width is $\Gamma_{qq}^{(0)} = \frac{3G_F m_q^2}{4\sqrt{2}\pi} m_h$, and including the $O(\alpha_s^2)$ and $O(\alpha_s^3)$ QCD corrections gives [59]

$$\Gamma_{qq} = \Gamma_{qq}^{(0)} K_{qq}, \qquad K_{qq} = \frac{\bar{m}_q^2(m_h^2)}{m_q^2}[1 + \Delta_{qq} + \Delta_H^2],$$
$$\Delta_{qq} = 5.67\frac{\bar{\alpha}_s}{\pi} + (35.94 - 1.36n_f)\frac{\bar{\alpha}_s^2}{\pi^2} + (164.14 - 25.77n_f + 0.26n_f^2)\frac{\bar{\alpha}_s^3}{\pi^3},$$
$$\Delta_H^2 = \frac{\bar{\alpha}_s^2}{\pi^2}\left(1.57 - \frac{2}{3}\log\frac{m_h^2}{m_t^2} + \frac{1}{9}\log^2\frac{\bar{m}_q^2}{m_h^2}\right), \tag{5.1}$$

where the running quark mass $\bar{m}_q(m_h^2)$, the strong coupling constant $\bar{\alpha}_s \equiv \alpha(m_h^2)$, and the light fermion flavor number n_f are defined at $\mu = m_h$ under $\overline{\text{MS}}$ scheme. For gluon gg final state, QCD corrections enhance the leading-order Higgs width $\Gamma_{gg}^{(0)}$ by a factor K_{gg} [59],

$$\Gamma_{gg} = \Gamma_{gg}^{(0)} \times K_{gg},$$
$$K_{gg} = 1 + \frac{215}{12}\frac{\bar{\alpha}_s(m_h^2)}{\pi} + \frac{\bar{\alpha}_s^2(m_h^2)}{\pi^2}\left(156.8 - 5.7\log\frac{m_t^2}{m_h^2}\right). \tag{5.2}$$

We have verified these formulas numerically and reached full agreement with [59]. For instance, in the mass range of $m_h = 100$–300 GeV, the QCD corrections amount to $K_{qq} \simeq 0.63$–0.39 for the qq final state, and $K_{gg} \simeq 1.87$–1.74 for the gg final state. With the above, we systematically summarize our calculations in Table V. From this table, we note that the Higgs boson $\hat{h}$ mainly decays to WW^* and $b\bar{b}$, with branching fractions equal to (15.7%, 20.9%, 35.8%) for WW^* channel and (61.7%, 56.5%, 33.2%) for $b\bar{b}$ channel, in sample-A, -B, and -C, respectively. On the other hand, we find that the Higgs boson $\hat{\chi}$ mainly decays to WW and ZZ channels for sample-A and -B, with decay branching fractions (72.8%, 61.5%) in WW channel and (26.8%, 26.9%) in ZZ channel. For sample-C, $\hat{\chi}$ dominantly decays to $b\bar{b}$ with a branching fraction 80.5%, while its decay branching ratios for the final states $\tau\bar{\tau}$, $c\bar{c}$, and gg equal 7.6%, 4.1%, and 2.8%, respectively.

Next, we study the production and decays of the visible Higgs bosons $\hat{h}$ and $\hat{\chi}$. The Higgs boson $\hat{h}$ is SM-like in the sense that its gauge and Yukawa couplings to WW/ZZ and $f\bar{f}$ are close to the SM values, but still can have sizable deviation in sample-A (cf. Table IV). It has a mass $m_h = (122, 125, 136)$ GeV in sample-A, -B, and -C, respectively. Its main production channel should be the gluon-gluon fusion with decays into two photons, $gg \to \hat{h} \to \gamma\gamma$. We also consider other two channel with the off-shell decays, $gg \to \hat{h} \to WW^*, ZZ^*$. For the on-shell production of $\hat{h}$, we compute the cross section times branching fraction of $\hat{h} \to \gamma\gamma$ or $\hat{h} \to VV^*$ ($V = W, Z$), relative to that of the SM Higgs boson with the same mass. This gives the ratios

$$U_{\phi h}^2 \frac{\text{Br}[\hat{h} \to \gamma\gamma]}{\text{Br}[h \to \gamma\gamma]_{\text{SM}}} \simeq (0.693, 0.964, 0.844), \tag{5.3a}$$
$$U_{\phi h}^2 \frac{\text{Br}[\hat{h} \to VV^*]}{\text{Br}[h \to VV^*]_{\text{SM}}} \simeq (0.693, 0.964, 0.844), \tag{5.3b}$$

for sample-A, -B, and -C, respectively. The two ratios in (5.3a) and (5.3b) exactly coincide for each sample

TABLE VI. Higgs signatures for the LHC discovery via fusion processes $gg \to \hat{h} \to \gamma\gamma, \hat{\chi}\hat{\chi}$ and $gg \to \hat{\chi} \to WW, ZZ, \hat{h}\hat{h}$. For each sample in every channel, the cross section times decay branching ratios are shown in units of fb. For the $\hat{h} \to \gamma\gamma$ channel, we also list the signal rates of the SM Higgs boson in parentheses for comparison.

$gg \to \hat{h}$ or $\hat{\chi}$		$\hat{h} \to \gamma\gamma$	$\hat{\chi} \to WW$		$\hat{\chi} \to ZZ$			$\to \hat{h}\hat{h}$ or $\hat{\chi}\hat{\chi}$
Final state		$\gamma\gamma$ (SM)	$\ell\nu\ell\nu$	$\ell\nu jj$	$\ell\ell jj$	$\ell\ell\nu\nu$	$\ell\ell\ell\ell$	$b\bar{b}b\bar{b}$
Sample-A	7 TeV	26.0 (37.5)	50.2	319	38.2	10.9	1.84	···
	14 TeV	84.3 (122)	195	1230	148	42.4	7.13	···
Sample-B	7 TeV	34.7 (36.0)	1.22	7.75	1.11	0.316	0.0532	0.233
	14 TeV	113 (118)	5.41	34.3	4.89	1.40	0.236	0.901
Sample-C	7 TeV	23.6 (28.0)	···	···	···	···	···	111
	14 TeV	79.2 (93.9)	···	···	···	···	···	373

since their left-hand-sides are actually equal due to $\Gamma[\hat{h} \to \gamma\gamma]/\Gamma[\hat{h} \to \gamma\gamma]_{\rm SM} = \Gamma[\hat{h} \to VV^*]/\Gamma[\hat{h} \to VV^*]_{\rm SM} = U^2_{\phi h}$. We see that for sample-A and -C, the $\hat{h}$ signals in $\gamma\gamma$ channel (and VV^* channels) are suppressed by 31% and 16% relative to that of the SM prediction, respectively, while the $\hat{h}$ signal rate is lower by 3.6% in sample-B. So, detecting our $\hat{h} \to \gamma\gamma$ signals in sample-A and -C is significantly *harder than that of the SM Higgs boson*, and it requires *higher integrated luminosity at the LHC*. The same statement is also true for our signals in $\hat{h} \to WW^*, ZZ^*$ channels. It is expected that with a total integrated luminosity of 10 fb^{-1} for two experiments at 7 TeV and combining all available channels, the SM Higgs boson exclusion will be extended to $m_h = 114$–600 GeV at 3σ level [60]. For sample-C, since $\hat{h}$ has a mass larger than twice of $\hat{\chi}$, we also have the decay channel $\hat{h} \to \hat{\chi}\hat{\chi} \to b\bar{b}b\bar{b}$, as will be discussed below.

Then, we consider the Higgs boson $\hat{\chi}$ which has a large P-odd component. The largest channels are still the gluon-gluon fusion processes: (i) $gg \to \hat{\chi} \to WW(ZZ)$ with $WW \to \ell\nu\ell\nu$, $\ell\nu jj$, or $ZZ \to \ell\ell jj$, $\ell\ell\nu\nu$, $\ell\ell\ell\ell$, for sample-A and -B, as shown in Fig. 5(a); (ii) and another reaction, $gg \to \hat{\chi} \to \hat{h}\hat{h}$ with $\hat{h}\hat{h} \to b\bar{b}b\bar{b}$, for sample-B, as illustrated in Fig. 5(b); and (iii) for sample-C, we consider the gluon-gluon fusion via $gg \to \hat{h} \to \hat{\chi}\hat{\chi}$ with $\hat{\chi}\hat{\chi} \to b\bar{b}b\bar{b}$, which is depicted in Fig. 5(c).

For each fusion process of Fig. 5, we have computed the production cross section of $\hat{h}$ and $\hat{\chi}$ for the relevant samples, by including the full next-to-leading order QCD corrections as in [59]. Then we multiply the production cross section by the decay branching fraction of each final state. For the final state decays into b jets, we have taken a b-tagging efficiency equal 60% [61] in our analysis; while for the final decay products being leptons, we will just select electrons and muons, $\ell = e, \mu$. We consider the LHC's center-of-mass energy at 7 TeV for the current run, and at 14 TeV for its next phase [62]. These are summarized in Table VI. For the $\hat{h} \to \gamma\gamma$ channel, we also list the results for the SM Higgs boson (with the same mass) in parentheses as a comparison. It shows that in sample-A and -C the $\hat{h}$ signal rates are lower than the SM Higgs boson by 31% and 14%, respectively. For the $\hat{\chi}$ production in the WW and ZZ channels, we find that the cross section times branching ratio has the following suppression relative to that of the SM Higgs boson with the same mass, for sample-A and -B,

$$U^2_{\phi\chi} \frac{\mathrm{Br}[\hat{\chi} \to WW]}{\mathrm{Br}[h \to WW]_{\rm SM}} \simeq (0.290, 0.0139), \tag{5.4a}$$

$$U^2_{\phi\chi} \frac{\mathrm{Br}[\hat{\chi} \to ZZ]}{\mathrm{Br}[h \to ZZ]_{\rm SM}} \simeq (0.301, 0.0141). \tag{5.4b}$$

This shows that the signal rate of $\hat{\chi}$ over that of the SM Higgs boson is 29–30% for sample-A and decreases to

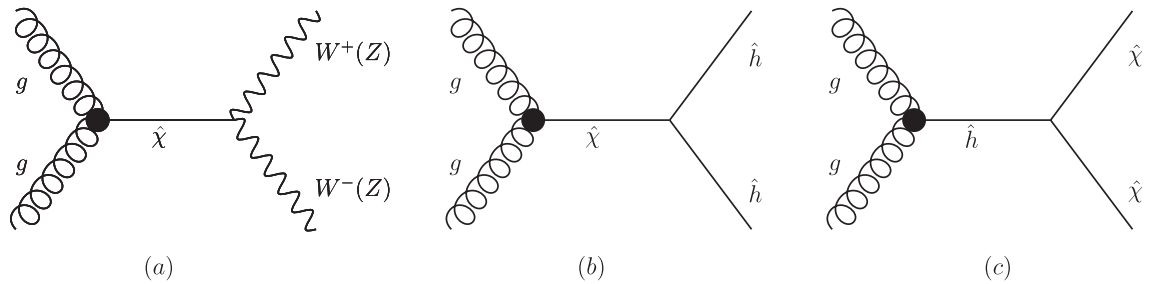

FIG. 5. Predicted new production processes of the Higgs boson via gluon-gluon fusions at the LHC. The diagram (a) is for sample-A; the diagrams (a) and (b) are for sample-B; and the diagram (c) is for sample-C. The big black dot denotes the gluon-gluon-Higgs vertex as contributed by the fermion and gauge triangle diagrams in each case.

about 1.4% for sample-B, in both WW and ZZ channels. So, detecting the new Higgs boson $\hat{\chi}$ in these channels will require higher integrated luminosities at the 7 TeV LHC. From Table VI, we see that the process $gg \to \hat{\chi} \to \hat{h}\,\hat{h} \to b\bar{b}b\bar{b}$ for sample-B has a lower rate and is hard to detect at the 7 TeV LHC; but the 14 TeV LHC will have a larger signal rate by a factor of 4.5. For sample-C, the $\hat{\chi}$ boson only weighs about 59.4 GeV, and thus the best channel should be $gg \to \hat{h} \to \hat{\chi}\,\hat{\chi} \to b\bar{b}b\bar{b}$, which has large signal rates even at the 7 TeV LHC, about 106 fb, as shown in Table VI. The major concern would be the SM $4b$ backgrounds, because the signal contains relatively soft b jets from the light $\hat{\chi}$ decays.

For this channel $gg \to \hat{h} \to \hat{\chi}\,\hat{\chi} \to b\bar{b}b\bar{b}$, we note that it may also be probed at Fermilab Tevatron, which has recorded about 10 fb^{-1} data in both CDF and D0 detectors by the end of summer 2011 [63]. For sample-C, we find the production cross section of $gg \to \hat{h}$ with $m_h = 136$ GeV to be about 736 fb at Tevatron. Including the decay branching fractions $\mathrm{Br}[\hat{h} \to \hat{\chi}\,\hat{\chi}] = 10.2\%$ and $\mathrm{Br}[\hat{\chi} \to b\bar{b}] = 80.5\%$, and a 60% b-tagging efficiency, we estimate the effective signal cross section to be 6.3 fb. For 10 fb^{-1} data, we would expect about 63 events for the $4b$ final states from this process in each detector, so we encourage the Tevatron colleagues to analyze such $4b$ events from their complete data set. But one should keep in mind that since sample-C predicts a rather light singlet Higgs boson $\hat{\chi}$ weighing about 59.4 GeV, the b jets in its decay products will be relatively soft, with energy less than 30 GeV and transverse momentum not much larger than 15–20 GeV. This differs a lot from the b jets out of direct $\hat{h}$ decays in the process of Fig. 5(b) for sample-B, where $\hat{h}$ weighs about 125 GeV and the resultant b jets are hard [64,65]. This makes it harder to reconstruct such a light $\hat{\chi}$ resonance of sample-C above the background b jets. At the LHC, the backgrounds with relatively soft b jets are expected to be larger and thus more challenging. We encourage systematical Monte Carlo analyses for both Tevatron and LHC detectors to optimize the signals of $gg \to \hat{h} \to \hat{\chi}\,\hat{\chi} \to b\bar{b}b\bar{b}$ and pin down their $4b$ backgrounds.

VI. DIRECT DETECTION OF GEV-SCALE MIRROR DARK MATTER

In this section, we first estimate the abundance of mirror helium dark matter [Sec. VI]. Then, we analyze direct detections of the GeV-scale mirror helium dark matter in Sec. VI, especially the new constraints from TEXONO [11] and the upcoming tests by CDEX [12]. We will study processes via the Higgs-exchange-induced scattering and the $\gamma - \gamma'$ mixing-induced scattering. We reveal that the cross section of $\gamma - \gamma'$ mixing-induced scattering is enhanced in the low recoil-energy region relative to that of the Higgs exchange, and is thus sensitive to direct detections.

A. Abundance of mirror helium dark matter

In the visible world, the lightest baryon is a proton, and after the ordinary BBN, matter will be mainly composed of ordinary hydrogen atoms. As discussed in Sec. III [cf. (3.50)], the temperature T' of the mirror world is lower than the corresponding temperature T in the visible world by about a factor of 2 after the electroweak phase transition. This will cause a significant difference in the mirror BBN. To be concrete, we know that before the mirror BBN, the mirror protons and neutrons will convert into each other via reactions $n' \leftrightarrow p' + e'^{-} + \bar{\nu}'_e$, $n' + \nu'_e \leftrightarrow p' + e'^{-}$, and $n' + e'^{+} \leftrightarrow p' + \bar{\nu}'_e$. As the Universe expands, the temperature decreases and the cross sections of these processes become smaller. When the reaction rate becomes comparable to the Hubble expansion rate H, these reactions will be frozen and the mirror neutrons will decay freely until the mirror BBN starts, during which the mirror protons and neutrons form the mirror nucleus. Let us denote the freeze-out temperature of the mirror sector as T'_f, then from the distribution of kinetic equilibrium we can infer the ratio between the number densities of mirror protons and neutrons at freeze-out,

$$\frac{n_{n'}}{n_{p'}} \simeq \exp\left(-\frac{\Delta m'}{T'_f}\right), \tag{6.1}$$

where the mass difference $\Delta m' = m_{n'} - m_{p'}$. The $n - p$ mass difference $\Delta m = m_n - m_p$ is mainly caused by the mass difference between the current quarks d and u, namely, $m_d - m_u \propto v_\phi$. Similarly, the $n' - p'$ mass difference $\Delta m'$ mainly arises from $m_{d'} - m_{u'} \propto v_{\phi'}$. Thus, we expect the ratio, $\Delta m'/\Delta m \sim v_{\phi'}/v_\phi \sim 1/2$, in our construction. Then, we need to estimate the freeze-out temperature T'_f for mirror protons and neutrons. We note that in the visible sector of the Universe, the neutrons and protons freeze out at the temperature $T_f \sim 0.8$ MeV [47]. Then, from the freeze-out to the start of BBN (at $T_{\mathrm{NUC}} \sim 0.1$ MeV), the neutrons decay freely in this period, and decrease the neutron-to-proton ratio from about $1/6$ to $1/7$. For the nucleosynthesis, essentially all neutrons combine with protons into ^{4}He; the resulting mass fraction of ^{4}He is [47]

$$Y_{\mathrm{He}^4} \simeq \frac{4(n_n/2)}{n_n + n_p} = \frac{2(n_n/n_p)_{\mathrm{NUC}}}{1 + (n_n/n_p)_{\mathrm{NUC}}} \simeq 25\%. \tag{6.2}$$

This means that the visible Universe is dominated by the hydrogens which have an abundance of about 75%. As mentioned above, in the mirror sector the equilibrium of mirror neutrons and protons is maintained by the β decay, inverse decay, and the collision process, among which the collision process is most relevant. The collision rate $\Gamma_{p'e' \to n'\nu'}$ (per nucleon per time) can be expressed as

$$\Gamma_{p'e'\to n'\nu'} = (\tau_{n'}\lambda_0)^{-1} \times \int_q^\infty dy \frac{y(y-q)^2(y^2-1)^{1/2}}{[1+\exp(yz)][1+\exp((q-y)z_{\nu'})]}, \tag{6.3}$$

where the ratios $q = \Delta m'/m_{e'}$, $y = E_{e'}/m_{e'}$, $z = m_{e'}/T'$, and $z_{\nu'} = m_{e'}/T_{\nu'}$. In (6.3), $\tau_{n'}$ is the mean lifetime of mirror neutrons,

$$\tau_{n'}^{-1} = \Gamma_{n'\to p'e'\bar{\nu}'} = \frac{G_F'^2}{2\pi^3}(1+3g_A'^2)m_{e'}^5\lambda_0, \tag{6.4}$$

where $\lambda_0 \equiv \int_1^q dy y(y-q)^2(y^2-1)^{(1/2)} \simeq 1.636$, and g_A' is the axial-vector coupling of the mirror nucleon. Since the mirror and visible strong forces have the same coupling strength as required by the mirror parity, we have $g_A' = g_A \simeq 1.26$. The collision rate (6.3) can be evaluated numerically, and in the high/low temperature limits, it is approximated as

$$\Gamma_{p'e'\to n'\nu'} = \begin{cases} \tau_{n'}^{-1}(T'/m_{e'})^3\exp(-\Delta m'/T'), & T' \ll \Delta m', m_{e'}, \\ \frac{7\pi}{60}(1+3g_A'^2)G_F'^2T'^5, & T' \gg \Delta m', m_{e'}, \end{cases} \tag{6.5}$$

similar to that for the visible sector [47]. Then, the freeze-out temperature T_f' can be estimated by matching the collision rate and the Hubble expansion rate,

$$\Gamma_{p'e'\to n'\nu'}(T_f') \sim H(T_f'), \tag{6.6}$$

where

$$H(T') = \sqrt{\frac{4\pi^3}{45}}\frac{g_*'^{1/2}T'^2}{M_{\rm Pl}}, \tag{6.7}$$

and g_*' is the effective relativistic massless degrees of freedom in the mirror sector, $g_*' = 10.75[1+(T/T')^4]$. For our construction $T/T' \simeq v_\phi/v_{\phi'}$ and $x \equiv v_\phi/v_{\phi'} = 2$, so we have $g_*' \simeq 182.75$. In the visible sector, we have $g_* = 10.75[1+(T'/T)^4] \simeq 11.4$ for $T'/T = 1/2$, where, as expected, the effective contribution from the mirror sector is mainly negligible. So, the condition $\Gamma_{pe\to n\nu}(T_f) \sim H(T_f)$ determines the freeze-out temperature of visible protons and neutrons, $T_f \sim 0.8$ MeV, as in the standard cosmology [47]. We further note that the Fermi constants in the visible and mirror sectors are connected by $G_F'/G_F = (v_\phi/v_{\phi'})^2$. Taking all these into account, we estimate the freeze-out temperature of the mirror neutrons and protons, $T_f' \sim 0.5$ MeV. With these, we can infer the mirror neutron-to-proton ratio at the freeze-out from Eq. (6.1),

$$\left(\frac{n_{n'}}{n_{p'}}\right)_{\text{freeze-out}} \simeq \exp\left(-\frac{\Delta m'}{T_f'}\right) \simeq 28\%. \tag{6.8}$$

Since the visible and mirror strong forces have the same strength, it is expected that the mirror nucleosynthesis starts at the same temperature as the visible sector (though at an earlier time), i.e., $T_{\rm NUC}' = T_{\rm NUC} \sim 0.1$ MeV. For the radiation-dominated epoch, we have $H(T') = (4\pi^3/45)^{1/2}g_*'^{1/2}T'^2/M_{\rm Pl}$ and $t = [2H(T')]^{-1}$. Thus, we can estimate the time from $T' = T_f' \sim 0.5$ MeV to $T' = T_{\rm NUC}' \sim 0.1$ MeV as $\Delta t \sim 17.2$ sec, which is less than half a minute. Using (6.4) for the lifetime of mirror neutrons and the corresponding formula for visible neutrons, we estimate $\tau_{n'}/\tau_n = (G_F/G_F')^2(m_e/m_{e'})^5 = v_\phi/v_{\phi'} = 2$, and thus $\tau_{n'} = 2\tau_n \simeq 1757$ sec. Thus, the fraction of decayed mirror neutrons from the freeze-out epoch to the nucleosynthesis epoch is about $1 - \exp(-\frac{17.2}{1757}) \simeq 0.97\%$, which is negligible. Hence, we have

$$\left(\frac{n_{n'}}{n_{p'}}\right)_{\rm NUC} \simeq \left(\frac{n_{n'}}{n_{p'}}\right)_{\text{freeze-out}} \simeq 28\%. \tag{6.9}$$

Finally, we can estimate the mass fraction of mirror helium ^{4}He$'$,

$$Y_{\rm He^{4\prime}} \simeq \frac{4(n_{n'}/2)}{n_{n'}+n_{p'}} = \frac{2(n_{n'}/n_{p'})_{\rm NUC}}{1+(n_{n'}/n_{p'})_{\rm NUC}} \simeq 44\%. \tag{6.10}$$

This shows that the mirror sector has a much larger amount of mirror helium than the ordinary helium in the visible sector [cf. (6.2)]. As we will analyze shortly, the ultra-low-energy germanium detectors of the TEXONO [11] and CDEX [12] experiments will be most sensitive to the mirror heliums as the dark matter particles, since they are significantly heavier than the mirror hydrogens.

Then, we estimate the mass of mirror helium dark matter. From Eq. (3.13), we can infer the ratio between the mirror and visible nucleon masses,

$$\frac{m_{N'}}{m_N} = \left(\frac{v_{\phi'}}{v_\phi}\right)^{2/9} \simeq 0.60\text{–}0.92, \tag{6.11}$$

where we have used VEV limit $0.1 < v_{\phi'}/v_\phi < 0.7$ in (3.34), which is based on the BBN constraint (3.51) and the naturalness condition (2.17). This means that the mirror helium ^{4}He$'$ should weigh about 60–92% of the ordinary ^{4}He, and thus has a mass around 3 GeV,

$$M_{\rm He^{4\prime}} \simeq (0.60\text{–}0.92)M_{\rm He^4} \simeq 2.3\text{–}3.5 \text{ GeV}, \tag{6.12}$$

where our sample value $v_{\phi'}/v_\phi = \frac{1}{2}$ corresponds to $M_{\rm He^{4\prime}} \simeq 0.86 M_{\rm He^4} \simeq 3.2$ GeV.

B. Direct detection of mirror helium dark matter

In this subsection, we study direct detection of the GeV-scale mirror helium dark matter, especially the new constraint from TEXONO [11] and the upcoming probe by CDEX [12]. We will study the Higgs-exchange-induced scattering process and the $\gamma - \gamma'$ mixing-induced scattering process, respectively.

We first analyze the direct detection of Higgs-exchange-induced scattering. As shown in (3.11), the mass of ordinary nuclei depends on the Higgs vacuum expectation value via $m_N \propto v_\phi^{2/9}(\Lambda_{(6)})^{21/27}$, so the coupling of the

Higgs boson with proton or neutron can be estimated [66] by using trace anomaly. One may shift the vacuum expectation value as $v_\phi \to v_\phi + \phi$, and consequently the Yukawa coupling of the Higgs boson with nuclei can be derived by variation,

$$\lambda_{\phi NN} = \frac{\partial m_N}{\partial v_\phi} = \frac{2m_N}{9v_\phi}. \tag{6.13}$$

Also, from the trace anomaly we have [67]

$$\lambda_{\phi NN} = \frac{1}{v_\phi}\left\langle N \left| \sum_q m_q \bar{q} q \right| N \right\rangle \equiv \frac{f m_N}{v_\phi}, \tag{6.14}$$

where the coefficient f characterizes the contribution of trace anomaly and may be varied in the range $0.14 < f < 0.66$, with a central value $f = 0.30$ [67]. This is consistent with (6.13), where we have $f = \frac{2}{9} \simeq 0.22$. Similar to (6.13), for the mirror Higgs coupling to the mirror nuclei, we can deduce from (3.12)

$$\lambda_{\phi' N' N'} = \frac{f' m_{N'}}{v_{\phi'}}, \tag{6.15}$$

with $f' = f = \frac{2}{9}$. In the following analysis we will set $f' = f = 0.3$ for simplicity. With the Yukawa couplings $\lambda_{\phi NN}$ and $\lambda_{\phi' N' N'}$ given above, we can estimate the scattering cross section of the mirror nucleus with the ordinary nucleus via Higgs exchange.

As shown earlier, we have estimated that, after the mirror BBN, the mirror dark matter mainly consists of the mirror helium $^4He'$ (with a mass fraction about 44%) and the mirror hydrogen H' (with a mass fraction about 56%). The mirror hydrogen is significantly lighter than the mirror helium according to (6.11) and (6.12), and thus harder to directly detect. Hence, we will consider the mirror $^4He'$ dark matter for the present analysis, and estimate its scattering cross section in the detector.

We derive the Higgs-exchange-induced differential cross section as follows:

$$d\sigma = \frac{1}{4\pi v_0^2}[\lambda_{\phi' p' p'} Z' + \lambda_{\phi' n' n'}(A' - Z')]^2 \left(\sum_i \frac{U_{\phi' i} U_{\phi i}}{m_{\phi_i}^2}\right)^2 \times [\lambda_{\phi pp} Z + \lambda_{\phi nn}(A - Z)]^2 F_{A'}^2(Q) F_A^2(Q) dQ^2, \tag{6.16}$$

where v_0 denotes the velocity of incident dark matter relative to the Earth, $(Z', A') = (2, 4)$ for mirror helium nucleus, and the subscript i runs over the scalar mass eigenstates. The function $F_A(Q)$ $[F_{A'}(Q)]$ is the form factor of ordinary [mirror] nucleus, defined as $F_A(Q) = \frac{3j_1(Qr_A)}{Qr_A} e^{-(1/2)(Qs)^2}$, where $s = 0.9$ fm, and $r_A \simeq 1.14 A^{1/3}$ [68]. Thus, it is found to monotonously increase as Q^2 decreases, and $F_A(Q), F_{A'}(Q) \to 1$ for $Q^2 \to 0$.

To compare with experiments of direct dark matter detection, we should normalize the above cross section to the cross section of mirror dark matter scattering on a proton. So we apply (6.16) and derive

$$d\sigma_p = \frac{1}{4\pi v_0^2} \lambda_{\phi pp}^2 [\lambda_{\phi' p' p'} Z' + \lambda_{\phi' n' n'}(A' - Z')]^2 \times \left(\sum_i \frac{U_{\phi' i} U_{\phi i}}{m_{\phi_i}^2}\right)^2 F_{A'}^2(Q) dQ^2 \simeq \frac{(\lambda_{\phi pp} \lambda_{\phi' p' p'} A')^2}{4\pi v_0^2} \left(\sum_i \frac{U_{\phi' i} U_{\phi i}}{m_{\phi_i}^2}\right)^2 dQ^2, \tag{6.17}$$

where in the second step we have used the relation $\lambda_{\phi' p' p'} \simeq \lambda_{\phi' n' n'}$ due to $m_{p'} \simeq m_{n'}$, as well as $F_{A'}^2(Q) \simeq 1$ due to $Q^2 \simeq 0$. Note that $Q < Q_{\max} = 2\mu_p v_0$, where $\mu_p \simeq 0.7$ GeV is the reduced mass of the ordinary proton with the mirror helium $^4He'$ dark matter particle, and v_0 is the dark matter velocity relative to the Earth. So, v_0 should be smaller than the sum of the dark matter's escape velocity ($\lesssim 650$ km/s) and the relative velocity of Sun ($\lesssim 230$ km/s) in the Milky Way. Thus, we can derive, $Q < Q_{\max} < 4.1$ MeV, for our case. We have numerically checked that for $A = 4$ and $Q \leq 5$ MeV, the form factor $F_A^2(Q) \geq 0.9991$ and thus $F_A(Q) \simeq 1$ holds to high accuracy. The form factor $F_{A'}(Q)$ for mirror nuclei should be similar, so we expect that $F_{A'}^2(Q) \simeq 1$ holds well for $A' = 4$ and $Q < 4.1$ MeV, in the case of mirror helium $^4He'$. Integrating over Q^2, we arrive at

$$\sigma_p \simeq \int_0^{Q_{\max}^2} dQ^2 \frac{d\sigma_p}{dQ^2} = \frac{\mu_p^2 (\lambda_{\phi pp} \lambda_{\phi' p' p'} A')^2}{\pi} \left(\sum_i \frac{U_{\phi' i} U_{\phi i}}{m_{\phi_i}^2}\right)^2, \tag{6.18}$$

where $Q_{\max} = 2\mu_p v_0$. Using the model parameters of sample-A, -B, and -C, we finally derive

$$M_{He^{4\prime}} \simeq 3.2\,\text{GeV}, \quad \sigma_p \simeq (1.4, 3.4, 7.6) \times 10^{-50}\,\text{cm}^2, \tag{6.19}$$

for sample-A, -B, and -C, respectively. The σ_p appears quite below the sensitivities of current dark matter direct search experiments.

Alternatively, we note that the mirror dark matter may also be detected via the $\gamma - \gamma'$ mixing term (2.6). The cross section of a mirror nucleus (A', Z') scattering on an ordinary nucleus (A, Z) is

$$d\sigma = \frac{4\pi \epsilon^2 \alpha^2 Z'^2 Z^2}{Q^4 v_0^2} F_{A'}^2(Q) F_A^2(Q) dQ^2. \tag{6.20}$$

Because of the Q^4 factor in the denominator, this differential cross section receives a large enhancement in the low recoil-energy region relative to the above cross section via Higgs exchanges. This will overcome the large ϵ^2 suppression in (6.20) since the $\gamma - \gamma'$ mixing parameter is subjects to the experimental limit $\epsilon < 3.4 \times 10^{-5}$ in Eq. (4.26). This may be used to explain [69–71], the recent results from DAMA/LIBRA [72], CoGeNT [73], and CRESST

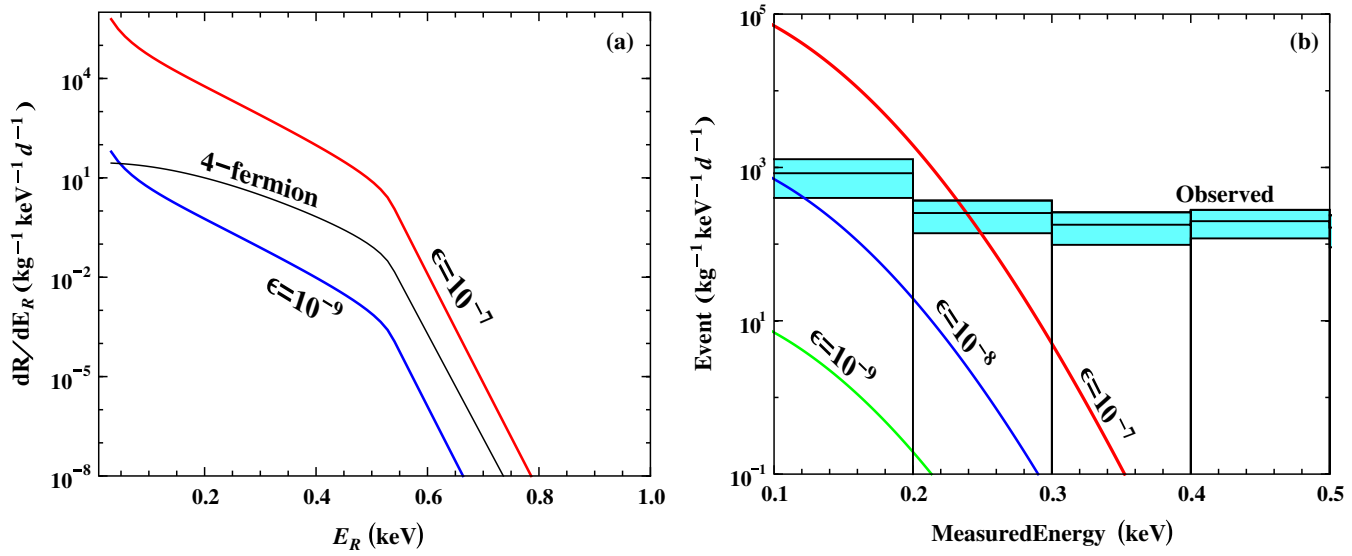

FIG. 6 (color online). Event rate distributions versus recoil energy. The plot in (a) shows the event rate distributions (in units of $\mathrm{kg}^{-1}\ \mathrm{keV}^{-1}\,\mathrm{day}^{-1}$) as a function of recoil-energy E_R (in keV), for two different values of the $\gamma - \gamma'$ mixing parameter ϵ (red and blue curves). As a comparison, the distribution from a 4-fermion interaction with an assumed $\sigma_p \simeq 10^{-38}\ \mathrm{cm}^2$ is shown by the black curve. The plot in (b) depicts the event rate distributions as a function of quenched recoil-energy, for three sample values of the mixing parameter ϵ. The observed event rate of TEXONO [11] is shown by the black histogram, and the shaded areas (light blue) are the experimentally allowed region within $\pm 1\sigma$ errors.

[74] experiments for dark matter detection. We further note that the ultra-low-energy germanium detectors of TEXONO [11] at Kuo-Sheng (KS) lab and of CDEX [12] at Jinping deep underground lab (CJPL) have a low recoil-energy threshold and are sensitive to the light dark matter in the 1–10 GeV mass range [12]. This should be an ideal place to look for the GeV-scale mirror dark matter as in (6.12), via the $\gamma - \gamma'$ mixing-induced scattering.

For our analysis, we simulate the event rate distributions over the recoil energy E_R for both $\gamma - \gamma'$ mixing-induced interaction and the usual 4-fermion interaction. We show the results in Fig. 6 for the event rate (in units of $\mathrm{kg}^{-1}\ \mathrm{keV}^{-1}\,\mathrm{day}^{-1}$) versus the recoil-energy (in keV), for germanium detectors. Since the mirror helium has the typical thermal energy (temperature) of O(keV), which is much larger than the ionization energy (about 20–50 eV) of the $^4\mathrm{He}'$ atoms, we expect that all the mirror helium atoms get ionized. So the mean mass of the particles composing the thermal mirror gas component of the halo should be about one third of the $^4\mathrm{He}'$ nuclei mass [75]. According to (6.12), we have chosen here a sample mirror dark matter mass as 3.2 GeV. The reduced mass for mirror helium with germanium is $\mu' \simeq 3.1$ GeV. So we have $Q < Q_{\max} = 2\mu' v_0 \simeq 18.2$ MeV, and for $A' = 4$, the mirror form factor $F^2_{A'}(Q) > 0.9879$. The form factor $F^2_A(Q)$ for germanium in (6.20) will be evaluated precisely. In Fig. 6(a), we have shown the rate distributions for the $\gamma - \gamma'$ mixing parameter $\epsilon = 10^{-7}$ (red curve) and $\epsilon = 10^{-9}$ (blue curve), respectively. For comparison, we have also plotted the distribution from a 4-fermion interaction with an assumed $\sigma_p \simeq 10^{-38}\ \mathrm{cm}^2$ (black curve). We see that for the low recoil-energy region, the event rate of $\gamma - \gamma'$ interaction is much larger than that of the 4-fermion interaction. The TEXONO experiment [11] already put stringent limits on both spin-independent and spin-dependent cross sections for dark matter mass around 3–6 GeV, where an energy threshold of (220 ± 10) eV was achieved at an efficiency of 50% with a four-channel ultra-low-energy germanium detector, each with an active mass of 5 g.

To compare with TEXONO detection [11], we show our simulated signals and the observed experimental data of TEXONO in Fig. 6(b). Here the energy quenching factor is 0.2 for the germanium detector, and the energy resolution is given by [11], $\Delta E = (18.64\sqrt{E} + 60) \times 10^{-3}$. In Fig. 6(b), we plot the predicted event rate distributions as a function of quenched recoil-energy, for three sample values of the mixing parameter $\epsilon = (10^{-7}, 10^{-8}, 10^{-9})$, in red, blue, and green curves, respectively. The observed event rate of TEXONO [11] is depicted by the black histogram, and the shaded areas (light blue) represent the experimentally allowed region within $\pm 1\sigma$ errors. From Fig. 6(b), we see that the red curve with $\epsilon = 10^{-7}$ is significantly above the experimental observation (black histogram with errors) around the threshold, and is thus already excluded by TEXONO data. But the blue and green curves in Fig. 6 are fully consistent with data. Using the TEXONO data [11], we can further derive a 2σ upper bound on the range of the $\gamma - \gamma'$ mixing parameter, $\epsilon < 2.7 \times 10^{-8}$. Our predictions can be further explored by the exciting ongoing CDEX experiment in Jinping [12].

Before concluding this section, we clarify two issues related to the mirror baryonic dark matter in general, although they are not particular to our present model. The first one concerns the stability of the dark halo. As the dark halo is assumed to be spherical and isothermal, if the dark matter is composed of mirror elements (mainly H' and He$'$), they would be ionized when the temperature T' is much higher than their ionization energy. Thus the bremsstrahlung and other processes can radiate off energies of the dark halo, so that it could not maintain its temperature T'. This is known as the radiative cooling problem. This issue can be resolved by a proper heating mechanism which prevents the collapse of the dark halo [4,76]. It was shown [76] that the energy released from both ordinary and mirror types of supernovas are candidates for such heating sources. Mirror supernovas can supply the energy if they occur at a rate of around one per year. Alternatively, ordinary supernovas can do the job to heat the mirror dark matter if the photon-mirror-photon kinetic mixing (2.6) is about $\epsilon \sim 10^{-9}$. This mixing can release a significant fraction of the total energy given by supernova explosions into $e'^{\pm}$ and γ', and these energies can be absorbed by the halo. In comparison with the visible sector, since the mirror sector has lower temperature ($T' < T$) and thus earlier mirror BBN, different light-element abundances, lighter particle masses ($m' < m$), and much larger dark matter density ($\Omega_{\rm DM} \simeq 5\Omega_{\rm B}$), there is *no macroscopic mirror symmetry*. So, it is quite expected that a significant asymmetry between the heating rates in both sectors exists, which can explain why the ordinary matter has collapsed into the disk and the mirror matter has not.

The second issue concerns structure formation of baryonic dark matter. The standard model of cosmology suggests that the early Universe is extremely homogeneous, while the large structures we see today (such as galaxies and clusters) arise from small primordial inhomogeneities that grow via gravitational instability. The primordial acoustic perturbation cannot grow until the recombination of the protons and the electrons, which occurs at a temperature around $T_{\rm dec} \simeq 0.25$ eV. (Prior to the photon decoupling, the radiation pressure prevents the growth of perturbations). But the study of the cosmic microwave background (CMB) shows that these perturbations do not have enough time to grow into galaxies. So the standard model cosmology requires the primordial perturbations of cold dark matter (instead of baryonic matter) to provide the seed of the large structure formation. For mirror models with unbroken mirror electromagnetism, mirror baryonic density can only begin to grow after mirror photon decoupling occurs (roughly at $T'_{\rm dec} \approx 0.25$ eV). But, as the BBN constraint requires $T' < T$, this means that mirror photons decouple *earlier* than the visible photons. It is shown [4,77] that for T' sizably below T, the large-scale structure formation with mirror dark matter closely resembles the conventional cold dark matter scenario. On the other hand, since mirror baryons can couple to visible photons through the $\gamma - \gamma'$ kinetic mixing, they become millicharged particles, having electric charges equal to ϵ times that of their visible partners. Thus, there is a possibility that electric force may suppress the primordial perturbation of the mirror baryons. As shown in [78] by using the CMB data, this imposes a constraint on the $\gamma - \gamma'$ mixing, $\epsilon < (4\text{–}6) \times 10^{-6}$, for the mirror baryonic dark matter in the mass range of 2–4 GeV. This is consistent with our model and is weaker than the limit derived from the direct detections in the above Fig. 6(b).

VII. CONCLUSIONS

The possible existence of a hidden mirror world in the Universe is a fundamental way to restore parity symmetry in weak interactions. It naturally provides the lightest mirror nucleon as a unique GeV-scale dark matter candidate.

We conjecture that *the mirror parity is respected by the fundamental interaction Lagrangian*, so its violation only arises from spontaneous breaking of the Higgs vacuum, and the possible soft breaking can only be linear or bilinear terms; we further conjecture that *all possible soft breakings simply arise from the gauge-singlet sector.* With this conceptually simple and attractive conjecture, we have studied spontaneous mirror parity violation in Sec. II, which quantitatively connects the visible and mirror neutrino seesaws with the common origin of CP violation. We presented systematical analysis of the minimal Higgs potential (2.8), which includes the visible/mirror Higgs doublets ϕ and ϕ' as well as a P-odd singlet scalar χ. The singlet χ develops a nonzero VEV v_χ at weak scale and generates $v_\phi \neq v_{\phi'}$ as in (2.15a) and (2.18c) [or (2.20)], leading to spontaneous breaking of the mirror parity (cf. Fig. 1). The domain-wall problem is resolved by a unique noninteracting soft-breaking term in (2.8b), and the usual vacuum degeneracy is removed (cf. Fig. 2). We have realized both the visible and dark matter geneses from a common origin of CP violation in the neutrino seesaw via leptogenesis (Sec. III). We presented two explicit seesaw schemes which generate successful visible and mirror leptogeneses with the common CP violation (as well as $\mu - \tau$ breaking) in Sec. III. We found that the right amounts of visible and dark matter densities ($\Omega_{\rm DM}$:$\Omega_{\rm M} \simeq 5$:1) are generated in the parameter space with a natural ratio of Higgs VEVs [cf. ((3.34))] and a proper mass ratio of singlet Majorana neutrinos [cf. (3.35)] between the visible and mirror sectors. The constraints from BBN on the visible and mirror sectors are further analyzed in Sec. III.

In Sec. IVwe analyzed the analytical parameter space of the model and explicitly constructed three numerical samples from the vacuum minimization, which predict distinctive Higgs mass spectrum and couplings, as shown

in Tables I, II, III, and IV and Fig. 1. We also studied in Sec. IV the low-energy direct and indirect constraints on the present model. We note that although the light mirror Higgs boson $\hat{h}'$ safely hides itself due to its small mixing of $O(10^{-2})$ with the visible Higgs $\hat{h}$, the P-odd singlet Higgs $\hat{\chi}$ (which generates unequal VEVs of $\hat{h}$ and $\hat{h}'$ and thus the spontaneous parity violation) has significant mixings with $\hat{h}$, as shown in (4.14). The Higgs boson χ is particularly light in sample-C and thus the LEP production channel $e^-e^+ \to Z\hat{\chi}$ (with $\hat{\chi} \to b\bar{b}$) is open. But we found that the sample-C prediction is well within the LEP Higgs search limit (Fig. 3). We further analyzed the indirect electroweak precision constraints via oblique corrections and found that the new contributions from our Higgs sector satisfy the precision $\Delta S - \Delta T$ limit in Fig. 4.

In Sec. V we further studied the distinctive new Higgs signatures of the predicted nonstandard Higgs bosons at the LHC. We systematically computed the Higgs decay widths and branching fractions for all three samples as summarized in Table V. Our construction always predicts a light mirror Higgs boson $\hat{h}'$, weighing about half of the $\hat{h}$ mass due to the VEV condition (3.34) with our sample value $v_{\phi'}/v_{\phi} = \frac{1}{2}$; but its mixing with $\hat{h}$ is only of $O(10^{-2})$ to satisfy the BBN constraint. So, different from all previous mirror models, the decay channel $\hat{h}' \to \hat{h}\,\hat{h}$ and its inverse process $\hat{h} \to \hat{h}'\hat{h}'$ are either forbidden or negligible. The mass of $\hat{h}$ lies in the range around 120–140 GeV, and its main LHC-production channel is $gg \to \hat{h}$ (with $\hat{h} \to \gamma\gamma$ and $\hat{h} \to VV^*$). As Eq. (5.3a) shows, relative to that of the SM Higgs boson, the $\hat{h}$ signal rate is suppressed by about (31%, 4%, 14%) in sample-A, -B, and -C, respectively. Besides, sample-C has a new production channel $gg \to \hat{h} \to \hat{\chi}\,\hat{\chi} \to 4b$ [Fig. 5(c)] with large signal rate at the LHC (Table VI), and is also potentially detectable at Tevatron. We encourage systematical Monte Carlo analyses to pin down the $4b$ backgrounds in this channel at both the LHC and Tevatron. For the P-odd Higgs boson $\hat{\chi}$, its main production channels are gluon-gluon fusions as shown in Figs. 5(a) and 5(b), besides Fig. 5(c), and its signal rates for each final state are summarized in Table VI. The $\hat{\chi}$ signal rates for both WW and ZZ final states are sizable at the 7 TeV and 14 TeV LHC, but as Eq. (5.4) shows, they are suppressed relative to that of the SM Higgs boson (with the same mass) by a factor about 29–30% and 1.4% in sample-A and -B, respectively. So, a higher integrated luminosity is required for their detection. The other fusion channel $gg \to \hat{\chi} \to \hat{h}\,\hat{h} \to 4b$ in Fig. 5(b) is open for sample-B, but with a relatively low signal rate as shown in Table VI. The approved LHC runs with 8 TeV collision energy [79]will further probe the predicted Higgs signals of our samples A, B, and C in this year.

Finally, in Sec. VI, we have studied direct detection of the mirror dark matter, which mainly consists of the mirror helium $^4\mathrm{He}'$ [with a mass fraction about 44% as estimated in (6.10)] and the mirror hydrogen H' (about 56%). The mass of mirror helium is around 3 GeV [cf. (6.12)]. Analyzing the scattering cross section of mirror helium with the nuclei in the (germanium or xenon) detector via Higgs exchanges shows that the signal is quite below the sensitivities of the current dark matter direct search experiments. But it is important to note that the $\gamma - \gamma'$ mixing-induced scattering is enhanced in the low recoil-energy region relative to that of the Higgs exchange [Fig. 6(a)]. We found that the TEXONO experiment [11] already puts nontrivial constraint on the parameter space of $\gamma - \gamma'$ mixing, as shown in Fig. 6. It reveals that the parameter region with $\gamma - \gamma'$ mixing $\epsilon \gtrsim 10^{-7}$ is significantly excluded by TEXONO; but the parameter space with $\epsilon < 2.7 \times 10^{-8}$ is fully consistent with TEXONO data at the 2σ level. The ongoing CDEX direct search experiment at CJPL deep underground lab also has a low recoil-energy threshold and is sensitive to the light dark matter in the mass range of 1–10 GeV [12]. It thus provides the ideal place to further explore the GeV-scale mirror dark matter. A summary of this work was presented in Ref. [80].

ACKNOWLEDGMENTS

We thank Robert Foot, Rabindra N. Mohapatra, Peihong Gu, Qaisar Shafi, and Raymond R. Volkas for valuable discussions, and Liang Han for discussing the LHC and Tevatron Higgs searches. We are also grateful to Henry Wong, Qian Yue, and Shin-Ted Lin for discussing the dark matter direct detections by the TEXONO [11] and CDEX [12] experiments, and especially to Henry Wong for providing us the original data of TEXONO [11] [used in our Fig. 6(b)], and to him and Shin-Ted Lin for explaining their analysis in [11]. H. J. H. thanks the Center for High Energy Physics at Peking University for kind support. This research was supported by the NSF of China (under Grants No. 10625522, 10635030, 11135003) and the National Basic Research Program of China (under Grant No. 2010CB833000), and by Tsinghua University. J. W. C. was supported in part by the China Postdoctoral Science Foundation (under Grant No. 20090460364).

Note added in proof.—After this work initially appeared in arXiv:1110.6893 on October 31, 2011, the ATLAS and CMS Collaborations announced new results for the Higgs searches at the LHC (7 TeV) on December 13, 2011 [81], which showed some interesting excesses of events for a Higgs boson mass around 125 GeV in the diphoton channel, although statistically inconclusive [79]. We have shown that a SM-like Higgs boson with mass about 125 GeV is just in the favored parameter space of the present model, as given by our sample-B (cf. Tables I and II). The Higgs boson weighs 122 GeV and 136 GeV in sample-A and -C, respectively. These

two samples predict significantly lower diphoton signals than the SM Higgs boson [cf. Eq. (5.3a)]. If the current excesses of events at the LHC (7 TeV) are disconfirmed by the upcoming data, our sample-A and -C can provide additional viable Higgs candidates. We expect that the new LHC runs at the collision energy of 8 TeV [79] will further test the predicted Higgs signals of both $\hat{h}$ and $\hat{\chi}$ in the samples-A, B, and C during this year.

[1] T. D. Lee and C. N. Yang, Phys. Rev. **104**, 254 (1956).

[2] I. Yu. Kobzarev, L. B. Okun, and I. Ya. Pomeranchuk, Sov. J. Nucl. Phys. **3**, 837 (1966); M. Pavsic, Int. J. Theor. Phys. **9**, 229 (1974); S. I. Blinnikov and M. Y. Khlopov, Sov. J. Nucl. Phys. **36**, 472 (1982); Sov. Astron. **27**, 371 (1983); S. L. Glashow, Phys. Lett. **167B**, 35 (1986).

[3] R. Foot, H. Lew, and R. R. Volkas, Phys. Lett. B **272**, 67 (1991); R. Foot and R. Volkas, Phys. Rev. D **52**, 6595 (1995); Z. Berezhiani and R. N. Mohapatra, Phys. Rev. D **52**, 6607 (1995); Z. Berezhiani, A. Dolgov, and R. N. Mohapatra, Phys. Lett. B **375**, 26 (1996).

[4] For nice reviews, R. Foot, Int. J. Mod. Phys. D **13**, 2161 (2004); L. B. Okun, Phys. Usp. **50**, 380 (2007); P. Ciarcelluti, Int. J. Mod. Phys. D **19**, 2151 (2010), and references therein.

[5] E. W. Kolb, D. Seckel, and M. S. Turner, Nature (London) **314**, 415 (1985).

[6] For example, H. M. Hodges, Phys. Rev. D **47**, 456 (1993); R. N. Mohapatra and V. L. Teplitz, Phys. Lett. B **462**, 302 (1999); Phys. Rev. D**62**, 063506 (2000); Z. Berezhiani, D. Comelli, and F. L. Villante, Phys. Lett. B **503**, 362 (2001); R. N. Mohapatra, S. Nussinov, and V. L. Teplitz, Phys. Rev. D **66**, 063002 (2002); A. Y. Ignatiev and R. R. Volkas, Phys. Rev. D **68**, 023518 (2003); Z. Berezhiani, P. Ciarcelluti, D. Comelli, and F. L. Villante, Int. J. Mod. Phys. D **14**, 107 (2005); P. Ciarcelluti, Int. J. Mod. Phys. D **14**, 187 (2005), and references therein.

[7] H. An, S. L. Chen, R. N. Mohapatra, and Y. Zhang, J. High Energy Phys. 03 (2010) 124.

[8] M. Fukugita and T. Yanagida, Phys. Lett. B **174**, 45 (1986).

[9] For a recent review, W. Buchmuller, R. D. Peccei, and T. Yanagida, Annu. Rev. Nucl. Part. Sci. **55**, 311 (2005), and references therein.

[10] Some models of spontaneous mirror parity violation were studied by R. N. Mohapatra and collaborators [6,7] in a very different context.

[11] S. T. Lin, H. B. Li, X. Li, S. K. Lin, H. T. Wong, M. Deniz, B. B. Fang, D. He, J. Li, C. W. Lin, F. K. Lin, X. C. Ruan, V. Singh, A. K. Soma, J. J. Wang, Y. R. Wang, S. C. Wu, Q. Yue, and Z. Y. Zhou (TEXONO Collaboration), Phys. Rev. D **79**, 061101 (2009).

[12] Q. Yue and H. T. Wong (CDEX-TEXONO Collaboration), arXiv:1201.5373; K. J. Kang, J. P. Cheng, Y. H. Chen, Y. J. Li, M. B. Shen, S. Y. Wu, and Q. Yue (CDEX Collaboration), J. Phys. Conf. Ser. **203**, 012028 (2010); H. T. Wong and S. T. Lin (TEXONO-CDEX Collaboration), Proc. Sci., ICHEP2010 (2010) 439.

[13] Ya. B. Zeldovich, I. Y. Kobzarev, and L. B. Okun, Sov. Phys. JETP **40**, 1 (1975); for reviews, A. Vilenkin, Phys. Rep. **121**, 263 (1985); T. W. B. Kibble, J. Phys. A **9**, 1387 (1976), and references therein.

[14] A. Salam and J. C. Pati, Phys. Rev. D **10**, 275 (1974); R. N. Mohapatra and J. C. Pati, Phys. Rev. D **11**, 566 (1975); G. Senjanovic and R. N. Mohapatra, Phys. Rev. D **12**, 1502 (1975).

[15] A. Y. Ignatiev and R. R. Volkas, Phys. Lett. B **487**, 294 (2000).

[16] R. Foot, H. Lew, and R. R. Volkas, Mod. Phys. Lett. A **7**, 2567 (1992); E. K. Akhmedov, Z. G. Berezhiani, and G. Senjanovic, Phys. Rev. Lett. **69**, 3013 (1992); R. Foot, Mod. Phys. Lett. A **9**, 169 (1994); R. Foot and R. R. Volkas, Phys. Rev. D **52**, 6595 (1995); R. Foot, M. J. Thomson, and R. R. Volkas, Phys. Rev. D **53**, R5349 (1996); Z. K. Silagadze, Phys. At. Nucl. **60**, 272 (1997); R. Foot and R. R. Volkas, Astropart. Phys. **7**, 283 (1997); M. Collie and R. Foot, Phys. Lett. B **432**, 134 (1998); R. R. Volkas and Y. Y. Y. Wong, Phys. Rev. D **58**, 113001 (1998); R. Foot and R. R. Volkas, Phys. Rev. D **61**, 043507 (2000); N. F. Bell, Phys. Lett. B **479**, 257 (2000); R. Foot and S. N. Gninenko, Phys. Lett. B **480**, 171 (2000); V. Berezinsky, M. Narayan, and F. Vissani, Nucl. Phys. **B658**, 254 (2003).

[17] B. Holdom, Phys. Lett. **166B**, 196 (1986); S. L. Glashow, Phys. Lett. **167B**, 35 (1986); E. D. Carlson and S. L. Glashow, Phys. Lett. B **193**, 168 (1987); R. Foot and X. G. He, Phys. Lett. B **267**, 509 (1991); S. Gninenko, Phys. Lett. B **326**, 317 (1994); R. Foot, A. Y. Ignatiev, and R. R. Volkas, Phys. Lett. B **503**, 355 (2001); S. V. Demidov, D. S. Gorbunov, and A. A. Tokareva, Phys. Rev. D **85**, 015022 (2012).

[18] R. S. Vallery, P. W. Zitzewitz, and D. W. Gidley, Phys. Rev. Lett. **90**, 203402 (2003).

[19] R. Foot, Int. J. Mod. Phys. A **19**, 3807 (2004).

[20] A. Badertscher, P. Crivelli, W. Fetscher, U. Gendotti, S. N. Gninenko, V. Postoev, A. Rubbia, V. Samoylenko, and D. Sillou, Phys. Rev. D **75**, 032004 (2007).

[21] P. Crivelli, A. Belov, U. Gendotti, S. Gninenko, and A. Rubbia, JINST **5**, P08001 (2010).

[22] For example, Z. G. Berezhiani, Acta Phys. Pol. B **27**, 1503 (1996) and references therein.

[23] For example, H. Casini and S. Sarkar, Phys. Rev. D **65**, 025002 (2001); B. Bajc, A. Riotto, and G. Senjanovic, Phys. Rev. Lett. **81**, 1355 (1998); G. Dvali and G. Senjanovic, Phys. Rev. Lett. **74**, 5178 (1995), and references therein.

[24] R. Foot, Int. J. Mod. Phys. D **13**, 2161 (2004).

[25] MACHO stands for massive astrophysical compact halo objects.

[26] C. Alcock *et al.* (MACHO Collaboration), Astrophys. J. **542**, 281 (2000).

[27] R. R. Uglesich, A. P. S. Crotts, E. A. Baltz, J. T. A. de Jong, R. P. Boyle, and C. J. Corbally, Astrophys. J. **612**, 877 (2004).

[28] P. Ciarcelluti, Int. J. Mod. Phys. D **19**, 2151 (2010).

[29] A. Mahdavi, H. Y. Hoekstra, A. Y. Babul, D. Y. Balam, and P. Capak, Astrophys. J. **668**, 806 (2007);

[30] M. J. Jee, A. Mahdavi, H. Hoekstra, A. Babul, J. J. Dalcanton, P. Carroll, and P. Capak, arXiv:1202.6368.

[31] Z. K. Silagadze, arXiv:0808.2595.

[32] A. D. Sakharov, Sov. Phys. JETP **5**, 24 (1967); for reviews, A. Riotto and M. Trodden, Annu. Rev. Nucl. Part. Sci. **49**, 35 (1999); M. Trodden, in *Proceedings of 32nd SLAC Summer Institute on Particle Physics (SSI 2004), Menlo Park, California, 2004*, eConf C040802, L018 (2004), and references therein.

[33] N. S. Manton, Phys. Rev. D **28**, 2019 (1983); V. Kuzmin, V. A. Rubakov, and M. E. Shaposhnikov, Phys. Lett. B **191**, 171 (1987); J. Ambjorn, T. Askgaard, H. Porter, and M. E. Shaposhnikov, Nucl. Phys. **B353**, 346 (1991).

[34] E. Komatsu *et al.* (WMAP Collaboration), Astrophys. J. Suppl. Ser. **192**, 18 (2011); O. Lahav and A. R. Liddle (Particle Data Group), J. Phys. G **37**, 246 (2010).

[35] Note that the ordinary lepton number and mirror lepton number are also softly broken by the singlet Majorana mass terms of heavy right-handed neutrinos and left-handed mirror neutrinos.

[36] J. A. Harvey and M. S. Turner, Phys. Rev. D **42**, 3344 (1990); S. Y. Khlebnikov and M. E. Shaposhnikov, Nucl. Phys. **B308**, 885 (1988).

[37] W. Buchmuller, P. Di Bari, and M. Plumacher, Ann. Phys. (N.Y.) **315**, 305 (2005); New J. Phys. **6**, 105 (2004); Nucl. Phys. **B643**, 367 (2002), and references therein.

[38] For a recent global fit of neutrino data, G. L. Fogli, E. Lisi, A. Marrone, A. Palazzo, and A. M. Rotunno, Phys. Rev. D **84**, 053007 (2011), and references therein.

[39] S.-F. Ge, H.-J. He, and F.-R. Yin, J. Cosmol. Astropart. Phys. 05 (2010) 017.

[40] H.-J. He and F.-R. Yin, Phys. Rev. D **84**, 033009 (2011).

[41] Y. I. Izotov and T. X. Thuan, Astrophys. J. **710**, L67 (2010); A. P. Serebrov, V. E. Varlamov, A. G. Kharitonov, A. K. Fomin, Yu. N. Pokotilovski, P. Geltenbort, I. A. Krasnoschekova, M. S. Lasakov, R. R. Taldaev, A. V. Vassiljev, and O. M. Zherebtsov, Phys. Rev. C **78**, 035505 (2008).

[42] Z. G. Berezhiani, A. D. Dolgov, and R. N. Mohapatra, Phys. Lett. B **375**, 26 (1996), and references therein.

[43] Z. Berezhiani, Int. J. Mod. Phys. A **19**, 3775 (2004).

[44] L. Knox and M. S. Turner, Phys. Rev. Lett. **70**, 371 (1993); see also, G. German, G. Ross, and S. Sarkar, Nucl. Phys. **B608**, 423 (2001); G. G. Ross and G. German, Phys. Lett. B **691**, 117 (2010).

[45] Since the expansion is much smaller here, a precise calculation will require the inclusion of radiation contribution to the Hubble constant in the phase transition epoch. But such detail is not needed for our discussion below.

[46] In our explicit minimization of the electroweak vacuum in Sec. IV, we will realize three sample patterns of the Higgs VEVs, $v_\chi \sim v_\phi \sim 2v_{\phi'}$ or $v_\chi \sim 4v_\phi \sim 8v_{\phi'}$.

[47] E. W. Kolb and M. S. Turner, *The Early Universe* (Addison-Wesley, Reading, MA, 1990).

[48] R. Barate *et al.* (ALEPH/DELPHI/L3/OPAL Collaborations) and (LEP Working Group for Higgs Boson Searches), Phys. Lett. B **565**, 61 (2003).

[49] M. E. Peskin and T. Takeuchi, Phys. Rev. D **46**, 381 (1992); Phys. Rev. Lett. **65**, 964 (1990).

[50] J. R. Forshaw, D. A. Ross, and B. E. White, J. High Energy Phys. 10 (2001) 007.

[51] K. Nakamura *et al.* (Particle Data Group), J. Phys. G **37**, 075021 (2010).

[52] M. E. Peskin and J. D. Wells, Phys. Rev. D **64**, 093003 (2001).

[53] W. J. Marciano, AIP Conf. Proc. **542**,48 (2000), and references therein.

[54] M. Baak, M. Goebel, J. Haller, A. Hoecker, D. Ludwig, K. Moenig, M. Schott, and J. Stelzer (The Gfitter Group), arXiv:1107.0975.

[55] A. Czarnecki, S. G. Karshenboim, in *Proceedings of the 14th International Workshop on High Energy Physics and Quantum Field Theory, (QFTHEP99)*, edited by B. B. Levchenko and V. I. Savrin (MSU-Press 2000 Moscow, Russia, 1999), p. 538.

[56] R. Barbieri, T. Gregoire, and L. J. Hall, arXiv:hep-ph/0509242; W. S. Li, P. F. Yin, and S. H. Zhu, Phys. Rev. D **76**, 095012 (2007); R. Foot, A. Kobakhidze, and R. R. Volkas, Phys. Rev. D **84**, 095032 (2011).

[57] A recent study [58] analyzed the LHC discovery of the Higgs portal from the SM to a hidden sector where the hidden Higgs boson mixes with the SM Higgs boson via the quartic interaction term.

[58] C. Englert, T. Plehn, D. Zerwas, and P. M. Zerwas, Phys. Lett. B **703**, 298 (2011); see also, C. Englert, J. Jaeckel, E. Re, and M. Spannowsky, Phys. Rev. D **85**, 035008 (2012).

[59] A. Djouadi, Phys. Rep. **457**, 1 (2008); A. Djouadi, J. Kalinowski, and M. Spira, Comput. Phys. Commun. **108**, 56 (1998), and references therein.

[60] A. Nisati (ATLAS Collaboration), "Higgs Searches in ATLAS," http://www.ino.tifr.res.in/MaKaC/getFile.py/access?contribId=115&sessionId=4&resId=0&materialId=slides&confId=79; V. Sharma (CMS Collaboration), "Search for the Higgs Boson with the CMS Detector," http://www.ino.tifr.res.in/MaKaC/getFile.py/access?contribId=116&sessionId=4&resId=0&materialId=slides &confId=79.

[61] S. Bhattacharya (CMS Collaboration), arXiv:1110.4569.

[62] For example, F. Bordry (LHC Team), "LHC Machine Status and Prospects," http://www.ino.tifr.res.in/MaKaC/materialDisplay.py?contribId=171&sessionId=31&materialId=slides&confId=79.

[63] M. Verzocchi (CDF Collaboration and D0 Collaboration), "Higgs Searches at the Tevatron," http://www.ino.tifr.res.in/MaKaC/getFile.py/access?contribId=117&sessionId=4&resId=0&materialId=slides&confId=79.

[64] For models with large $\hat{h}b\bar{b}$ Yukawa couplings, the $\hat{h}b\bar{b}$ associate production process is useful at the Tevatron and LHC [65]. There the $\hat{h} \to b\bar{b}$ decays generate much harder b jets since $\hat{h}$ usually has its mass obey the LEP limit, $m_h > 114.4$ GeV.

[65] U. Aglietti, A. Belyaev, S. Berge, A. Blum, R. Bonciani, J. Cammin, M. Carena, S. Chivukula, H. Davoudiasl, S.

Dawson, *et al.*, arXiv:hep-ph/0612172; M. Carena, J. S. Conway, H. E. Haber, J. D. Hobbs, *et al.*, arXiv:hep-ph/0010338; C. Balazs, J. L. Diaz-Cruz, H.-J. He, T. Tait, and C.-P. Yuan, Phys. Rev. D **59**, 055016 (1999), and references therein.

[66] M. A. Shifman, A. I. Vainshtein, and V. I. Zakharov, Phys. Lett. B **78**, 443 (1978).

[67] A. Bottino, F. Donato, N. Fornengo, and S. Scopel, Astropart. Phys. **13**, 215 (2000); M. M. Pavan, I. I. Strakovsky, R. L. Workman, and R. A. Arndt, PiN Newsletter **16**, 110 (2002); S. Andreas, T. Hambye, and M. H. G. Tytgat, J. Cosmol. Astropart. Phys. 10 (2008) 034.

[68] J. Engel, Phys. Lett. B **264**, 114 (1991); J. D. Lewin and P. F. Smith, Astropart. Phys. **6**, 87 (1996).

[69] R. Foot, Phys. Rev. D **82**, 095001 (2010); Phys. Lett. B **692**, 65 (2010); AIP Conf. Proc. **1178**, 111 (2009); arXiv:1110.2908.

[70] H. An, S. L. Chen, R. N. Mohapatra, S. Nussinov, and Y. Zhang, Phys. Rev. D **82**, 023533 (2010).

[71] N. Fornengo, P. Panci, and M. Regis, Phys. Rev. D **84**, 115002 (2011).

[72] R. Bernabei, P. Belli, F. Cappella, R. Cerulli, C. J. Dai, A. d'Angelo, H. L. He, A. Incicchitti, H. H. Kuang, X. H. Ma, *et al.* (DAMA Collaboration), Eur. Phys. J. C **67**, 39 (2010); **56**, 333 (2008); Riv. Nuovo Cimento **26**, 1 (2003).

[73] C. E. Aalseth, P. S. Barbeau, J. Colaresi, J. I. Collar, J. Diaz Leon, J. E. Fast, N. Fields, T. W. Hossbach, M. E. Keillor, J. D. Kephart, *et al.* (CoGeNT Collaboration), Phys. Rev. Lett. **107**, 141301 (2011); **106**, 131301 (2011).

[74] G. Angloher *et al.* (CRESST Collaboration), arXiv:1109.0702.

[75] R. Foot, arXiv:astro-ph/0403043.

[76] R. Foot and R. R. Volkas, Phys. Rev. D **70**, 123508 (2004).

[77] A. Y. Ignatiev and R. R. Volkas, Phys. Rev. D **68**, 023518 (2003); Z. Berezhiani, D. Comelli, and F. L. Villante, Phys. Lett. B **503**, 362 (2001).

[78] S. D. McDermott, H.-B. Yu, and K. M. Zurek, Phys. Rev. D **83**, 063509 (2011).

[79] CERN lately announced that the LHC will run at a center of mass energy of 8 TeV for this year; see ''LHC to Run at 4 TeV Per Beam in 2012,'' http://press.web.cern.ch/press/PressReleases/Releases2012/PR01.12E.html; see also, ''LHC Performance Workshop—Chamonix 2012,'' http: //indico.cern.ch/conferenceDisplay.py?confId=170230.

[80] J.-W. Cui, H.-J. He, L.-C. Lu, and F.-R. Yin, arXiv:1203.0968; Int. J. Mod. Phys. A **10**, 21 (2012).

[81] G. Aad *et al.* (ATLAS Collaboration), Phys. Lett. B **710**, 49 (2012); S. Chatrchyan *et al.* (CMS Collaboration), arXiv:1202.1488; F. Gianotti (ATLAS Collaboration), ''Update on the Standard Model Higgs Searches in ATLAS,'' http://lpsc.in2p3.fr/atlas/bclement/M2Particules/ATLAS-Higgs.pdf; G. Tonelli (CMS Collaboration), ''Update on the Standard Model Higgs Searches in CMS'', http://indico.cern.ch/getFile.py/access?contribId=1&resId=0&materialId=slides&confId=164890.